General Disclaimer

One or more of the Following Statements may affect this Document

- This document has been reproduced from the best copy furnished by the organizational source. It is being released in the interest of making available as much information as possible.

- This document may contain data, which exceeds the sheet parameters. It was furnished in this condition by the organizational source and is the best copy available.

- This document may contain tone-on-tone or color graphs, charts and/or pictures, which have been reproduced in black and white.

- This document is paginated as submitted by the original source.

- Portions of this document are not fully legible due to the historical nature of some of the material. However, it is the best reproduction available from the original submission.

NASA CR 72680
AMS T 903

1969 Summary Of Combustion Instability Research At Princeton University

by

L. Crocco, D. T. Harrje, W. A. Sirignano,
F. V. Bracco, A. P. Chervinsky,
C. B[illegible]o, T. J. Rosfjord, P. K. Tang,
J. S. T'i[illegible], T. S. Tonon, A. K. Varma, J. S. Wood

PRINCETON UNIVERSITY

prepared for

NATIONAL AERONAUTICS AND SPACE ADMINISTRATION

NASA Lewis Research Center
Grant NGL 31-001-115
Marcus Heidmann, Project Manager
Chemical Rockets Division

Requests for copies of this report should be referred to

National Aeronautics and Space Administration
Scientific and Technical Information Facility
P.O. Box 33
College Park, Md. 20740

NASA CR 72680
AMS T 903

1969 SUMMARY OF COMBUSTION INSTABILITY RESEARCH AT PRINCETON UNIVERSITY

by

L. Crocco, D. T. Harrje, W. A. Sirignano
F. V. Bracco, A. P. Chervinsky,
C. Bruno, T. J. Rosfjord, P. K. Tang
J. S. T'ien, T. S. Tonon, A. K. Varma, J. S. Wood

PRINCETON UNIVERSITY
DEPARTMENT OF AEROSPACE AND MECHANICAL SCIENCES
Princeton, New Jersey 08540

prepared for

NATIONAL AERONAUTICS AND SPACE ADMINISTRATION

February, 1970

GRANT NGL 31-001-155

NASA Lewis Research Center
Cleveland, Ohio
Marcus Heidmann, Project Manager
Chemical Rockets Division

TABLE OF CONTENTS

TABLE OF CONTENTS - CONT'D

ABSTRACT

Eight studies on the control and cause of combustion instability in rocket combustors are reported: 1) Acoustic Liner Theory, 2) Theoretical Study of Quarter-Wave Tubes, 3) Oscillatory Droplet Wake Diffusion Flames, 4) Combustion Response to Step-Shock Waves, 5) Unsteady Thermal Behavior of the Liquid Droplet, 6) Improved Mathematical Techniques for Nonlinear Oscillations, 7) Chemical Kinetic Effects and 8) Hydrogenation Rocket Feasibility Study. Each is extensively abstracted with regard to recent results and progress.

I. SUMMARY

Eight research topics on the control and cause of combustion instability in rocket engines studied at Princeton University during 1969 under a continuing NASA Grant are extensively abstracted.

Theoretical and experimental studies of the parameters governing Helmholtz resonator and quarter-wave tube damping efficiency are described. Improved methods for estimating flow effects are discussed and the quarter-wave tube damping mechanism is further explained. Companion studies involve sources of combustion instability and include: An actual combustion environment as influenced by the passage of a step-shock - major changes occur close to the injector. Droplet wake burning is simulated by an oscillating diffusion flame - preferred frequencies (resonance) intensify the combustion. Temperature profile within a droplet is treated analytically - this "skin" effect indicates improved chances for coupling. Improved mathematical techniques are being employed to solve the nonlinear equations associated with combustion instability. Chemical kinetic effects as well as a hydrogenation rocket were also investigated.

II. INTRODUCTION

This report summarizes the research into the methods of controlling combustion instability and into the underlying causes for the phenomena performed at Princeton University during 1969 under a continuing NASA Grant. Eight specific studies are reported. Each is presented in an extended abstract or condensed formal report format. When appropriate, the reader is referred to a more thorough reporting of the material presented herein. The purpose of this report is to present both the recent developments in instability research and a composite picture of the scope of the research conducted at Princeton.

A major portion of the research effort is in the area concerned with damping combustion driven oscillations. Helmholtz resonators, or liners when the resonators are used in great numbers, offer an attractive means of damping chamber pressure oscillations. One problem is that flow across the entrance to the resonator, or steady flow through this orifice, alters the frequency at which the resonator is most effective. Every chamber experiences flow effects. Using the jet flow model and adding the flow effects, equations which predict the new conditions are presented and discussed.

Another means of damping pressure oscillations utilizes the quarter-wave tube. A variety of designs can be contemplated. The mechanism for damping is discussed and the governing equations derived for this approach. The jet-flow model again is used to describe the basic mechanism.

Considering the sources of energy necessary to "drive" the resonant combustion, several areas of active study are described.

After determining the steady-state combustion environment associated with like-impinging injector designs both theoretically and experimentally, a step-shock (shock wave followed by a uniform pressure) is being used diagnostically in the unsteady program. The strength of the shock is recorded as it approaches the near region of injection; also studied are the changes in the uniform pressure step. Marked changes in the shock amplitude are limited to the region close to the injector. The degree of energy addition governs whether the oscillation will continue.

Jet burning, such as with co-axial injector elements, and the burning in the wake of a propellant droplet form the basis for the jet diffusion flame experiment and the closely related analytical studies. A laminar fuel jet is burned in an oscillating oxidizer environment. At a well-defined frequency, combustion is enhanced and the flame shortens and broadens its profile. Thermocouple and other probes, together with shadowgraph records, document the observations. The significant

findings both analytically and experimentally offer one explanation for the instability coupling mechanism.

The nonlinear oscillations in an annular combustion chamber are examined by analytical means. The rate-controlling process is assumed to be the Priem-Heidmann type of droplet vaporization. A considerable effort was required to determine the proper perturbation approach.

Another analytical study involving droplets considers the temperature nonuniformity from the cooler center to a thin vaporization temperature skin. The analysis points out increased peaking of pressure amplitude as frequency is varied compared to the uniform temperature droplet.

Chemical kinetic factors were investigated with regard to the preferred resonant combustion spin direction observed with different fuels. Data indicated consistent trends which confirmed spin effects but showed the chemical-kinetic factors to be of secondary importance for liquid-propellant rockets.

In the realm of different propulsion concepts hydrogenation of monopropellant decomposition was studied. The aim was to determine the feasibility of designing a high performance, low temperature engine with afterburning capability.

III. ACOUSTIC LINER THEORY

INTRODUCTION

Presently, one of the most effective ways to combat the undesirable effects of high-frequency combustion instability in liquid propellant rocket engines, and of high-intensity noise generation in air-breathing jet engines, is through the use of acoustic liners of the Helmholtz-resonator type. Up to now, a combination of acoustic theory and experimental data have been used to guide the configurations, however, these approaches have not proven to be very efficient in making such selections. An improved design procedure is one based on an accurate quantitative description of the actual flow situation and thereby guide the designer to the optimum liner configuration. This section describes the important analytical advances that have been made concerning these devices in this research program. First,the treatment of the resonator itself is described, and then some practical conclusions are discussed. Some of these advances have been reported in the literature[1, 2, 3, 4].

DETERMINING THE RESONATOR'S RESPONSE UNDER GIVEN CONDITIONS

The treatment of the resonator has been considered under two separate situations, namely, near-resonance and off-resonance. In all treatments, the jet-flow model is incorporated, i.e., a model which assumes that jet-type flow is representative of the nonlinear regime of resonator operation.[1] The off-resonance solution includes the effects of finite, external pressure fluctuations, and external velocity effects. The near-resonance solution considers, in addition, the effects of a mean flow through the orifice. Both studies allow the orifice length to be comparable to the wavelength of oscillation; but in addition, the mean conditions, the ratio of specific heats, and the molecular weight in the cavity must be essentially equal to the corresponding values in the chamber. The near-resonance solution reduces to the

quasi-steady solution when the orifice motion becomes quasi-steady. In this special case, a coefficient of discharge for the orifice is incorporated into the analysis. The chamber flow in these studies includes both a mean part and an oscillatory part. The angle between the flow direction of both parts is arbitrary, although the angle must be a constant. The phase angle between the oscillatory part of the velocity and the chamber oscillatory pressure is likewise considered arbitrary and constant.

A third analysis has been performed which considers large variations in mean conditions, in the ratio of specific heats, and in the molecular weight between the fluid in the cavity and that in the external environment. This latter study is valid only when the orifice motion is quasi-steady, and it considers only the effects of oscillatory pressure, with no velocity effects.

BOUNDARY EFFECTS AND OPTIMUM DAMPING

In a paper by Cantrell and Hart[5], an expression for the growth rate of first-order disturbances, within a volume enclosed by a surface, is derived. The results of this derivation can be applied, in first approximation, to the resonator problem. The enclosing surface must be properly defined, any transients must be slow compared to the period of oscillation, and there must be no significant coupling between the action of the liner and any combustion phenomena or other related phenomena present in real situations. When it is assumed that all of the mean and oscillatory flow quantities at the surface are small, and of the same order, the following may be concluded. First, from the results of this derivation, the optimum damping occurs in moving towards resonance (a perhaps obvious conclusion). Second, under near-resonance situations, a relatively simple surface integral is obtained, which is to be maximized for optimum instability damping. In special cases, this latter surface integral will be maximized when the real part of the admittance coefficient,

$\mathcal{Y}_R$, is maximized.* These cases include the following:

1) All modes if there is no mean flow in the chamber, and in addition, either no mean flow through the liner, or $\sigma^2 << 1$.

2) Transverse modes with either no mean flow through the liner or $\sigma^2 << 1$.

3) Longitudinal modes in which the chamber oscillatory velocity is 90^o out of phase with the chamber pressure, and if the orifice oscillatory velocity is in phase with the chamber pressure, and in addition, if either there is no mean flow through the orifice, or if $\sigma^2 << 1$.

DESIGN PROCEDURE

The design procedure is to maximize the surface integral mentioned previously, making use of the solutions to the resonator problem. In most practical situations, this amounts to maximizing $\mathcal{Y}_R$. In other words, if the conditions in the chamber are known, one can determine the proper liner geometry which will give the maximum damping. This determination can include flow effects (both through and past), differences in fluid conditions between the cavity and external environment, and an orifice length which is comparable to the wavelength. As indicated above, not all of these effects can be combined simultaneously. With this as a background, more detail can be added together with physical interpretations of interest to the designer, which will aid in understanding liner operation.

---

* We note that, from the above solutions for the resonator response, $\mathcal{Y}_R$ depends significantly upon the chamber flow terms and any mean flow through the orifices, so that these flow effects do influence the optimum liner geometry.

MAXIMIZATION OF $\mathcal{Y}_R$

As mentioned above, there are certain situations in which the optimum design is achieved when $\mathcal{Y}_R$ is maximized. For these situations in which the mean flow through the orifices is zero, the calculations involved in optimizing $\mathcal{Y}_R$ are greatly simplified. Now,

$$\mathcal{Y}_R = \bar{c}_1 \sigma M / \epsilon^{1/2} \bar{p}_1 \qquad (1)$$

where $\bar{c}_1$ is the mean speed of sound, σ is the percent open area ratio, M is a constant which becomes a maximum in a region close to resonance, ϵ is the amplitude of the non-dimensional, oscillatory chamber pressure, and $\bar{p}$ is the mean pressure. Thus, in the special cases of concern here, one should maximize both σ and M. When there is no mean flow through the orifices, the resonator geometry which gives the maximum value of M is given by*

$$AL/\mathcal{V} = \tilde{\omega} \tan \tilde{\omega} + \epsilon^{1/2} \tilde{\omega} \kappa / \pi M \cos^2 \tilde{\omega} \qquad (2)$$

where

$$\kappa = \frac{2}{3} bg (1 - \bar{C}_p) + \pi \bar{V}_1 g \cos\psi (\bar{C}_p + 1)/2 \qquad (3)$$

$$M^2 = 3 C_D^2 [\pi/\gamma + (\bar{V}_1^2 + 2b^2/3 + g^2/3)(1 - \bar{C}_p) + \pi \bar{V}_1 b \cos\psi (\bar{C}_p + 1)/2]/2 (1 + \cos^3\tilde{\omega}) \qquad (4)$$

and where A is the orifice cross-sectional area, L is the orifice length, $\mathcal{V}$ is the cavity volume, $\tilde{\omega} = 2\pi L/\lambda$,

---

* That M will be a maximum with this geometry has not been proven rigorously; however, calculations show that M will be at least approximately a maximum with this geometry. This geometry actually requires that the orifice velocity be in phase with the chamber oscillatory pressure.

λ the wavelength, $\bar{C}_p$ the average pressure coefficient the orifice jet "feels" upon entrance into the chamber, C_D is the discharge coefficient for the orifice in quasi-steady flow (in unsteady flow, $C_D = 1$), and the chamber pressure and velocity are assumed known in the following forms:

$$p_1 / \bar{p}_1 = 1 + \epsilon \cos \omega t \tag{5}$$

$$\vec{v}_1 / \bar{c}_1 = \vec{\bar{v}}_1 + \vec{v'}_1 \tag{6}$$

with the magnitudes,

$$\left| \vec{\bar{v}}_1 \right| = \epsilon^{1/2} \bar{v}_1 \tag{7}$$

$$\left| \vec{v'}_1 \right| = \epsilon^{1/2} b \cos \omega t + \epsilon^{1/2} g \sin \omega t \tag{8}$$

where $\bar{v}_1$, b, and g are constants of order unity, and ψ is the angle between the direction of $\vec{\bar{v}}_1$ and $\vec{v'}_1$ when both vectors are greater than zero.

The expressions (2-4) omit consideration of any differences in mean or gas properties across the orifice. It can be proven that a chamber flow will always increase the value of M given above, if $\bar{C}_p < 0$. Experimental evidence and physical reasoning suggest that $\bar{C}_p$ can only be negative. When the chamber flow terms are zero, the geometry given above becomes the Helmholtz-resonant geometry with no end correction applied to the orifice length. No end correction appears here since the flow fields exterior to the orifice were assumed to be quasi-steady. When fluid motion is quasi-steady, the fluid particles experience no acceleration in time, and thus no inertia is present.

In certain volume-limited situations, it is not possible to vary the liner geometry such that both M and σ are maximized independently. In these situations, when the cavity volume is fixed, the maximum value of γ_R will appear at a frequency above which M is a maximum. The precise optimum condition should then be found by direct calculation,

making use of a more general form of the solution not presented here. The reasoning which leads to this conclusion has been presented in Reference 2.

In certain situations, the chamber conditions are not known precisely enough to allow confidence in a design geometry calculated as described. In other cases, it is desirable to restrict the orifice length to a value much less than a wavelength. In both cases a quasi-steady flow situation should be induced in the orifice flow. The reason is that (with this restriction on the orifice length) the curve of M vs. the orifice length is quite flat (while other parameters are adjusted so that the curve lies near the resonant point), and the quasi-steady case, at resonance, affords a value very close to the largest that can be obtained. The added advantage is that (in the quasi-steady regime) the resonator response is insensitive to the orifice length, i.e., the acoustic effective length of the orifice is zero. When the K-factor in Equation (3) is zero, the quasi-steady-resonant point is achieved by making the orifice length as small as possible, and the cavity volume as large as possible. The approach is asymptotic so that some sloppiness in design can be permitted. If the K-factor is not zero, then there exists a certain finite, optimum, cavity volume and/or non-zero, optimum, orifice length. Thus, more care must be taken in selecting the liner geometry, which can still be found from Equation (2). The orifice length to diameter ratio should always be kept large enough so that the flow will reattach to the walls of the orifice prior to exiting. It is found that the presence of a vena-contracta, without reattachment, limits the mass flow through the orifice, and thus lessens efficiency in these special cases where $\mathcal{Y}_R$ should be maximized.

When a mean flow is present in the orifice, the calculation of the optimum geometry involves the numerical solution of simultaneous algebraic equations.

PHYSICAL INTERPRETATION OF A CHAMBER FLOW

In this section, any mean flows through the orifice are omitted and the mean conditions and gas properties in the cavity are considered equal to those in the external environment.

Resistance can be defined as the force which leads to the dissipation, divided by the orifice velocity. In the jet-flow regime, this resistance will be a function of time, illustrating the nonlinear character of the motion. It can be shown, however, that an effective linear resistance can be found, which is constant for a given periodic motion. The following expression for resistance can be derived from these concepts.

$$R_0 = (2/3\pi)\,\bar{\rho}\,\hat{u}\,(1 + \alpha^3) \tag{9}$$

where R_0 is the equivalent linear resistance per unit orifice area, ρ is the density, $\hat{u}$ the amplitude of the orifice velocity at one end of the orifice, which is used in the definition of R_0, and α is the ratio of the orifice velocity amplitude at the far end of the orifice to $\hat{u}$. A phase difference between the velocities at the two ends of the orifice does not enter into the expression. In quasi-steady flow, the result can be extended to include certain real flow effects, and becomes

$$R_0 = (4/3\pi C_D^{\,2})\,\bar{\rho}\,\hat{u} \tag{10}$$

where C_D is the coefficient of discharge for the orifice (which includes vena-contraction and frictional effects), and $\hat{u}$ is the orifice velocity amplitude averaged over the orifice cross-sectional area. From the analysis, it is found for the real part of the impedance Z_R (the impedance is defined as the ratio of the chamber pressure oscillation to the normal velocity oscillation near the liner), that

$$Z_R = R_0/\sigma + F(\omega, \omega_r, \hat{u}, \vec{V_1}) \tag{11}$$

where the function F need not be written explicitly here, but $F(\omega, \omega_r, \hat{u}, 0) = 0$. Thus, the real part of the impedance equals the resistance only when the chamber flow effects are absent. The interpretation of this is that the part of the chamber pressure in phase with the orifice velocity does not precisely supply the force which is dissipated (that force which accelerates the fluid particles from rest to the orifice-jet velocity). Thus, both the chamber pressure and velocity fields must be considered as forcing functions for the gas motion in the orifice (i.e., the chamber velocity field modifies the actual working-force associated with the orifice motion). From this fact, one can realize that the chamber velocity field can influence the phase angle between the orifice velocity and the chamber oscillatory pressure; and one could suspect that there are certain regions where this phase angle is such that the orifice velocity works against the chamber oscillatory pressure. Indeed, calculations show that in the presence of a chamber flow, $\mathcal{Y}_R$ (or Z_R) can be negative. In these latter regions, and in those situations mentioned earlier where $\mathcal{Y}_R$ should be made large for stability, the liner will certainly enhance instability. Energy from the chamber velocity field then does work on the chamber pressure field. These regions, of course, must be avoided, and the resonator geometry which gives the boundary between $\mathcal{Y}_R$ positive and negative can be found from an expression very similar to Equation (2), although it will not be given here. M (and $\mathcal{Y}_R$) can only be positive in using Eqs. (2-4).

In some experimental studies found in the literature, the resistance is defined as the real part of the impedance, even when a chamber flow is present. Such a definition does not account for the physical mechanisms just described.

IV. THEORETICAL STUDY OF QUARTER-WAVE TUBES

INTRODUCTION

In the development of acoustic liners for the suppression of rocket combustion instability, Helmholtz resonators have been at the center of interest. There are some other types of damping devices which have good potential but have not yet been explored in great detail. The purpose here is to study a particular device which is often referred to as a quarter-wave tube. It is intended to determine if this device can absorb the energy of chamber pressure oscillations effectively. Construction of the quarter-wave tube is quite simple; it is a slender tube of circular section with one end closed and the other end connected to the rocket combustor or the fan duct in the case of jet engines. The length of the tube is one-quarter of the wavelength of the oscillation for which the tube is designed to absorb. At the tuned frequency, the wave travelling from the entrance of the tube to the end and reflecting back to the entrance will arrive with opposite phase to another incoming wave. The interference between these two waves results in the attenuation of pressure oscillations. In addition, the velocity oscillation inside the tube is large, particularly near the tuned frequency (resonance), and any dissipative mechanisms which are related to the velocity such as viscous effects and kinetic dissipation, also play important roles in reducing the oscillation and broadening the response. Figure 1 is a schematic diagram of the quarter-wave tube.

FIGURE 1

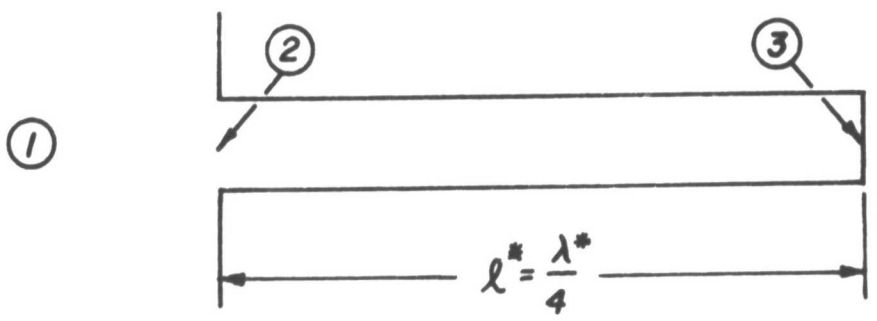

Several assumptions are made in the study of the quarter-wave tube: 1) the flow inside the tube is one-dimensional, 2) frictional losses and heat transfer are negligible, 3) the principle damping mechanism involves the loss of jet kinetic energy when the flow emerges from the tube into the chamber (this is called the jet-flow model), 4) the entropy is essentially constant (the production of entropy due to the kinetic energy loss of the jet is neglected since the gas volume in the chamber is much larger than the gas flow in the tube), and 5) the gas is thermally and calorically perfect.

Before writing the governing equations for the gas flow, the boundary conditions should be discussed. At the tube end where a solid wall condition is assumed, the gas velocity u must be zero. At the tube entrance, the boundary condition is far more complicated and therefore must be given much more attention. For flow into the tube, the chamber and tube entrance conditions can be connected through the quasi-steady isentropic relation. This can be justified if the time required for the condition at the tube entrance to respond to the change in the chamber conditions is much shorter than the characteristic time of change (i.e., the period of oscillation). Should this not be the case, a more complicated flow pattern must occur in that region. After nondimensionalizing all quantities by the mean chamber condition, for flow into the tube, the boundary condition appears as

$$c_2^+ = p_1^{\frac{\gamma - 1}{\gamma}} \left[\frac{1 - W_2^2}{1 - W_1^2}\right]^{1/2} \qquad (1)$$

where c, p, and γ represent the speed of sound, pressure and specific heat ratio. W is the ratio of gas velocity to the maximum of gas velocity which the stream could attain locally and has the form of

$$W^2 = \frac{\gamma - 1}{2} \left(u^2/p_1^{\frac{\gamma - 1}{\gamma}}\right)/\left(1 + \frac{\gamma - 1}{2} u_1^2/p_1^{\frac{\gamma - 1}{\gamma}}\right) \qquad (2)$$

subscripts 1 and 2 denote the conditions in the chamber and at the tube entrance, respectively. Superscript + indicates that the condition is valid only for flow into the tube.

The situation for flow into the chamber is completely different. Due to the dissipation of the kinetic energy of the jet, no isentropic relation can be applied. This is because the jet dynamic pressure, which is related to the kinetic energy, cannot be recovered. In order to establish certain relations between the chamber and the tube entrance, a pressure coefficient C_p is introduced. This can be visualized as a certain cross flow in the chamber over a cylinder formed by the jet column. Without the cross flow, i.e., with no chamber flow, the pressure in the chamber is the same as that at the tube entrance. With cross flow, C_p is usually taken as the average value of the local pressure coefficient over the circumference of the jet. (If the jet column were effectively a solid body and the Mach number of the chamber flow is small, then C_p would be -1 for a perfect fluid and even smaller for a real fluid.) Hence the boundary condition for outward flow may be written as

$$c_2^- = [p_1 + \frac{1}{2} C_p \gamma p_1^{\frac{1}{\gamma}} V_1^2]^{\frac{\gamma-1}{\gamma}} \qquad (3)$$

superscript - is the condition for outward flow only.

The governing equations are considered next. Two differential equations are needed, the continuity and momentum equations. The energy equation is replaced by the isentropic relations. In the nondimensionalization, the tube length and the period of oscillation in the chamber are chosen as the characteristic length and time. The mean speed of sound in the chamber is the characteristic velocity. Furthermore, there is another time of interest, namely, the period of resonance of the fundamental mode and it is defined as

$$t_{rs}^* = \frac{4\ell^*}{\bar{c}^*} \qquad (4)$$

where * denotes dimensional quantities, and, t^*_{rs} is the time required for the wave to travel four times the length of the tube ℓ^* (since this is a quarter-wave tube). A frequency ratio f is also defined which is the ratio of the frequency of the oscillation frequency tc the resonant frequency. The continuity and momentum equations, in dimensionless forms, are:

$$\frac{f}{4}\frac{\partial c}{\partial t} + u\frac{\partial c}{\partial x} + \frac{\gamma-1}{2}c\frac{\partial u}{\partial x} = 0 \qquad (5)$$

$$\frac{f}{4}\frac{\gamma-1}{2}\frac{\partial u}{\partial t} + \frac{\gamma-1}{2}u\frac{\partial u}{\partial x} + c\frac{\partial u}{\partial x} = 0 \qquad (6)$$

c and u are chosen as the two dependent variables. The advantages of selecting c and u as dependent variables give us some flexibility in the application of boundary conditions and will be seen later. Combination of (5) and (6) yields:

$$\frac{f}{4}\frac{\partial}{\partial t}\left(c + \frac{\gamma-1}{2}u\right) + (c+u)\frac{\partial}{\partial x}\left(c + \frac{\gamma-1}{2}u\right) = 0 \qquad (7a)$$

$$\frac{f}{4}\frac{\partial}{\partial t}\left(c - \frac{\gamma-1}{2}u\right) - (c-u)\frac{\partial}{\partial x}\left(c - \frac{\gamma-1}{2}u\right) = 0 \qquad (7b)$$

The above equations with the boundary conditions mentioned earlier can be solved analytically by using a perturbation method. Details will be seen in the next two sections.

SOLUTION: OFF-RESONANCE

In the study of the off-resonance case, all quantities are expanded into power series of a small parameter ϵ which is the amplitude of pressure oscillation in the chamber. The following orders are assigned for various quantities:

$$p_1 = O(\epsilon) \; ; \; V_1 = O(\epsilon) \; ; \; u = O(\epsilon)$$
$$c = O(\epsilon) \qquad (8)$$

Omitting the details of the analysis, the final result will be presented here. A time-averaged acoustic admittance is defined as

$$\mathcal{Y} = \left\langle \frac{u_2^{(1)} + \epsilon u_2^{(2)}}{p_1^{(1)}} \right\rangle \tag{9}$$

where $\langle\ \rangle$ is the time average over a period. The real part of $\mathcal{Y}$ is

$$\mathcal{Y}_R = \frac{\epsilon}{\pi} \left| \tan \frac{\omega}{4} \right| \left\{ \frac{2}{3\gamma^2} \left| \tan \frac{\omega}{4} \right|^2 \right.$$

$$- \left[\frac{\pi}{2} \bar{V}_1 \cos\psi\, V_1' S_1 \right] (1 + C_p) \tag{10}$$

$$\left. - \left[\left(\bar{V}_1^2 + \frac{V_1'^2}{2} \right) + \frac{V_1'^2}{6} (S_1^2 - C_1^2) \right] (1 - C_p) \right\}$$

which is of order ϵ since the contribution from $u_2^{(1)}$ is zero. The imaginary part is

$$\mathcal{Y}_I = -\frac{1}{\gamma} \left| \tan \frac{\omega}{4} \right| \sin \delta_2$$

$$- \epsilon \frac{1}{\pi} \left| \tan \frac{\omega}{4} \right| \left\{ \left[\frac{\pi}{2} \bar{V}_1 \cos\psi\, V_1' C_1 \right] (1 + C_p) \right.$$

$$\left. + \left[\frac{2}{3} V_1'^2 S_1 C_1 \right] (1 - C_p) \right\} \tag{11}$$

$\mathcal{Y}_R$ is also called the response and is related to the dissipative effect. The first term on the right-hand-side of (10) is attributed to the jet loss and its effect is dominating when operation is near resonance. On the other hand, $\mathcal{Y}_R$ becomes zero when f is an even integer, including zero. In the region where f is close to an even integer, the velocity effect can be significant and negative response may result. Rocket designers must apply this kind of knowledge intelligently

so that maximum response can be obtained and thus favorable attenuation can result.

SOLUTION: NEAR-RESONANCE

From the off-resonance study, it is found that the velocity amplitude at the tube entrance becomes infinity when the frequency of the pressure oscillation in the chamber approaches the resonant frequency of the tube. This violates the small perturbation assumption and thus the result cannot be applied in that region. Physically, the oscillation cannot become infinite since some dissipative effect will limit the growth. In this problem, the jet energy loss is thought to be the only dissipative agent. The oscillation will reach a maximum when the work done on the gas by the pressure oscillation is balanced by the dissipation. The jet kinetic energy loss is proportional to the velocity squared (i.e., order u_2^2). From the Bernoulli relation, the pressure amplitude in the chamber must be of the same order as u_2^2. Assuming u is of order ϵ, then

$$p_1 = O(\epsilon^2) \tag{12}$$

To achieve the same order of oscillation amplitude inside the tube as that in the off-resonance case, the pressure amplitude is no longer of order ϵ but instead of order ϵ^2 in the near-resonance study. The reordering of p_1 modifies the boundary conditions at $x = 0$. The details of the analysis will not be presented here. Some algebraic equations result and an iteration method must be used to determine certain constants (A's and B's) under various conditions. The time average of the acoustic admittance is:

$$\mathcal{Y} = \mathcal{Y}_R + i\mathcal{Y}_I = \left\langle \frac{u_2^{(1)}}{p_1^{(2)}} \right\rangle \tag{13}$$

where

$$\mathcal{Y}_R = \frac{1}{\epsilon} [A_2 \cos \delta_2 + B_2 \sin \delta_2] \tag{14}$$

and

$$\gamma_I = \frac{1}{\epsilon}\left[B_2 \cos\delta_2 - A_2 \sin\delta_2\right] \qquad (15)$$

δ_2 is the phase between $u_2^{(1)}$ and $p_1^{(2)}$. The quarter-wave tube has now been solved analytically for both the near- and off-resonance cases. Further results will be forthcoming upon the completion of the numerical computations. The admittance coefficients as functions of frequency and the pressure and velocity waveforms will be calculated.

EXPERIMENTAL PROGRAM

The experimental program, which closely relates to the analytical studies just described, and the analysis listed under Acoustic Liner Theory, is providing important data that is directly influencing the theoretical effort. A subsequent report will cover the experimental progress in detail. Preliminary indications are that cavity shape may directly influence the breakup of the jet and hence influence the kinetic energy dissipation. Optical studies now in progress should supply data to more fully describe the events.

V. MASS, MOMENTUM AND ENERGY SOURCES

INTRODUCTION

Although much has been theorized on the processes that constitute steady and unsteady combustion, basic information on energy release rates in liquid rocket combustors is still limited. This research, through a combination of theoretical and experimental endeavors, is seeking data on the functional forms of the mass, momentum and energy sources present in such combustors under steady and unsteady one-dimensional operation. Such a direct effort to investigate these sources can provide important information and thereby achieve further progress in the understanding of combustion instability and of reactive two phase flows.

The approach used in this research relies on the fact that gasdynamic equations can be written for the flow associated with a shock wave in a gas with mass, momentum and energy sources. If the functional forms of the sources are known, the motion of the shock can be calculated; whereas if the motion of the shock is known, the functional forms of the sources can be investigated. The purpose of this research is to measure the critical parameters of a shock wave moving within a liquid rocket engine and to "exchange" these data for information on the functional forms of the sources themselves.

The program is divided into two parts. The steady-state sources are investigated in the first part and the unsteady state sources are investigated in the second. Both parts make direct use of experimental data. Generally the measured data are: static pressures and particle and shock velocities with streak records of the gas flow used as a check. A step-shock wave, generated by a shock tube positioned downstream of a radial nozzle, is used to investigate unsteady sources. The wave travels upstream into the high intensity combustion zone where the measurements are taken.

The conventional way of investigating a physical problem is that of i) formulating a model for it, ii) solving the corresponding equations and then iii) comparing the theoretical solution with experimental results. Alternatively one can follow a different approach in which the above three steps are rearranged. Namely, one can i) measure certain quantities, ii) solve basic equations using the measured quantities, and then iii) look for the proper model. The first method is the conventional one while the second will be referred to here as the "direct" one. The direct method seems to be the more natural one, particularly for complicated physical problems, since it squeezes the maximum information out of a set of experimental data. In the past, the direct method has been used occasionally, but more as a device to solve a specific problem rather than as a general method with associated characteristics, advantages and disadvantages.

The following seven properties of the direct method were isolated and will be discussed in detail in the forthcoming Ph.D. thesis and report of F.V. Bracco:[6]

1) Experimental data information optimization
2) Experimental data check
3) Mathematical simplification
4) Set splitting
5) Parameterization
6) Assumption splitting
7) Maximum information

STEADY-STATE COMBUSTION

The steady-state combustion of the LOX-ethanol system was thoroughly investigated by the direct method. The method itself could be applied to the study of other propellants. Also, a number of the conclusions can be extended to other propellant systems. A specific knowledge of steady-state combustion is essential for any realistic study of unsteady combustion. The prime measured parameter was the static pressure. From these measurements it was possible to calcu-

late the steady-state gas velocity, density, temperature, composition and mass, momentum, and energy sources without using any drag, vaporization or distribution for the drops. The gas velocity thus calculated was then checked by direct measurements using streak techniques in three different engine configurations, and the agreement was found to be good.

A parametric study of the system of equations was then completed and has provided answers to such relevant questions as:

- The validity of the assumption of chemical equilibrium of the combustion products
- The relationship between mass and energy sources
- The degree of steady-state axial uniformity
- The influence of axial nonuniformity on the frequency of longitudinal acoustic waves
- The importance of the initial momenta of the liquids
- The relative magnitude of droplet drag and vaporization effects on the momentum equation of the gas

Also, a set of simplified equations which describe the steady state were determined and should be of use in numerical instability studies. The above points and other related discussions are found in the Bracco thesis and report.[6]

Finally, after having determined the gas parameters, several droplet drag vaporization and distribution models were studied for a specific LOX-ethanol engine configuration (the results were presented at the 6th ICRPG Conference[7]). In conducting this investigation simpler models were considered first. The simpler the model, the better the possibilities for steady and unsteady applications.

It was first assumed that all drops have initially the same radius and burn according to one of the following

four burning rate equations:

$$\frac{dr}{dt} = -\frac{K_1}{8r} \tag{1a}$$

$$\frac{dr}{dt} = -\frac{K_2}{8r}\left[1 + .276\ Pr^{1/2}\ Re^{1/2}\right] \tag{2a}$$

$$\frac{dr}{dt} = -\frac{K_3}{8r}\ Re^{1/2} \tag{3a}$$

$$\frac{dr}{dt} = -\frac{K_4}{8r}\ Re \tag{4a}$$

(1) where:

$$Re = \frac{2r\rho\,|V - V_\ell|}{\mu}$$

$$Pr = \frac{4\gamma}{9\gamma - 5}$$

Both the no drag (drops moving at constant speed) and the drag cases (Stokes' drag equation) were studied. None of these models gave satisfactory agreement. However a drag equation, weaker than the Stokes' type, would have made this model acceptable.

A Nukiyama-Tanasawa initial distribution function for the drops was then selected and the spray equation was then solved using the assumption of Stokes' drag for each of the above four burning rate equations. First the coefficients K_1, K_2, K_3 and K_4 were set equal to constants. With the selection of proper values for these constants, the agreement was found marginally acceptable for all four burning rate equations. In all cases the overall combustion rate tended to be too fast near the injector and too slow far from it. The method of solution was such that it was possible to evaluate the influence of a selected burning rate equation and drag model on the drop distribution function without specifying the actual drop distribution function at $x = 0$.

Next the coefficients K_1, K_2, K_3, and K_4 were taken to be proportional to the gas temperature; actually the inverse of the density was used. The results are as follows:

$$\frac{dr}{dt} = -\frac{K_1}{\rho 8r} \tag{1b}$$

$$\frac{dr}{dt} = -\frac{K_2}{\rho\ 8r}\left[1 + .276\ Pr^{1/3}\ Re^{1/2}\right] \tag{2b}$$

$$\frac{dr}{dt} = -\frac{K_3}{\rho\ 8r}\ Re^{1/2} \tag{3b}$$

$$\frac{dr}{dt} = -\frac{K_4}{\rho\ 8r}\ Re \tag{4b}$$

where: K_1, K_2, K_3, and K_4 are constants

All four models then gave good agreement. Due to a lower gas temperature near the injector and a higher value downstream, the combustion rates were reduced in the vicinity of the injector and increased far from it, thus bringing about a proper agreement. Of the above four burning rate models, the third,(3b),could possibly be selected as that giving a slightly better agreement. However, the fourth, (4b), would yield a greater mathematical simplicity which is always desirable for instability studies.

One more set of models was studied. A Nukiyama-Tanasawa initial drop distribution function was again selected and the spray equation was solved but with the further assumption of no drag (all drops at constant speed). The second and third of the four burning rate equations with K_2, and K_3 again equal to proper constants (no temperature dependence) gave again good agreement. Due to a lower relative velocity near the injector and to a higher one far from it, the combustion rates were reduced in the vicinity of the injector and increased far from it, thus again bringing about the proper agreement, although this last set of models is physically not quite correct, it again offers the advantage of mathematical simplicity without losing in overall accuracy.

The conclusion of this study is that several droplet spray, burning and drag models have been found by which the overall combustion in the engine could accurately be predicted. However, using also the findings of other researchers, specifically on the problem of jet breakup, of drop burning under forced convection and of drag on burning drops, one would conclude that the most consistent overall description of the combustion in the engine under consideration is obtained with a Nukiyama-Tanasawa initial drop distribution function, a Stokes' drag and a Spalding's burning rate equation (the third equation) with a coefficient proportional to the local gas temperature (or inversely proportional to the local gas density) multiplying $R_e^{1/2}$. The proportionality constant may have to be determined experimentally as in the case of the engine

studied. In the actual Spalding's burning rate equation the factor multiplying $R_e^{1/2}$ is a specific function of temperature, but the conditions of Spalding's experiments are too far from those of a real engine to expect the same temperature dependence. The simplified models, which still gave the same overall good agreement, should prove useful in steady and unsteady combustion studies.

UNSTEADY COMBUSTION

An experimental engine - shock tube apparatus has been used to study the unsteady mass-energy source. The apparatus is shown in Fig. 2 and consists of the combustion chamber with an extension to allow the step-shaped-shock generated from the shock generator to develop fully prior to entering the important combustion region. The gathering of the experimental data for the determination of unsteady energy sources has proven to be quite difficult. In mid 1969 the hardware was redesigned to avoid two problems which had surfaced with the previous set up. These two problems were the incomplete formation of the step-shock (initiated from the shock tube) before its entrance into the combustion zone, and a chamber Mach number that was too low and resulted in poor resolution of the velocity data. With the new hardware extensive testing was done toward the end of 1969 and early 1970. At this time a complete set of experimental data is available but the most noticeable feature of these data is that the step-shock is found to undergo drastic changes in the region near the injector face. Hence some additional information then becomes desirable for that specific location. A description of the experimental apparatus, procedure and data reduction will be presented in the Master's thesis of S.N. Narayanan which should become available later this year.

The theoretical and computational part needed to go from the measured static pressure after the shock front ($p = p(x,t)$) to the unsteady mass-energy source ($Q = Q(x,t)$)

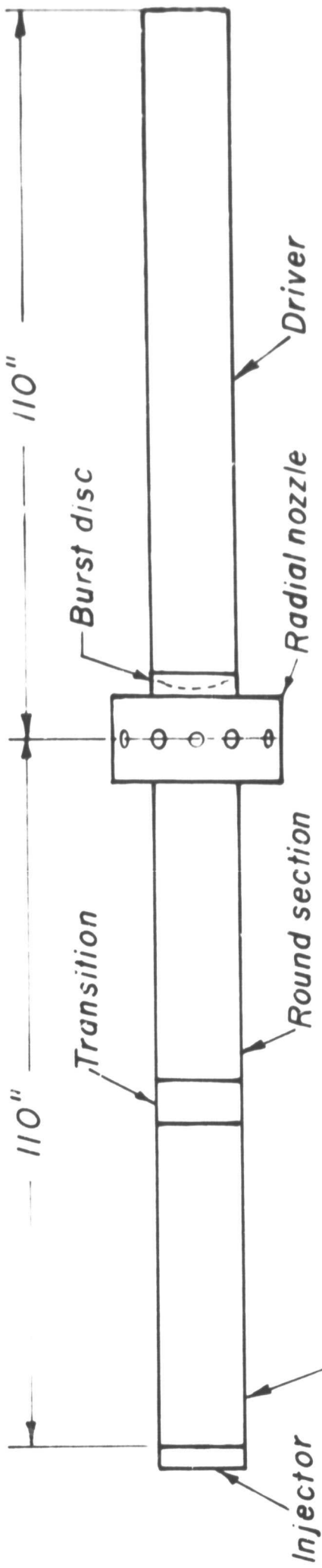

Rocket for step-pulse shock studies

Figure 2

was completed in the summer of 1969. It is composed of two parts. In the first part, the shock front conditions are solved (under both equilibrium composition and frozen flow assumptions) using the previously discussed steady-state calculations and by measuring shock front pressure. In the second part, the solution for the shock region is numerically obtained with the final determination of $Q = Q(x,t)$, $\rho = \rho(x,t)$ and $u = u(x,t)$ thus accomplished. Although the above computational tools have long been available, their validity and accuracy cannot be finally tested until complete experimental data become available. A study of $Q = Q(x,t)$ in light of the n, τ model is also planned. A report, and possibly some journal publications, about these unsteady computations will be prepared by F.V. Bracco upon completion of the task.

VI. OSCILLATORY FREE DIFFUSION FLAMES AND UNSTEADY DROPLET BURNING

INTRODUCTION

In the study of combustion instability in liquid propellant rocket motors, it has been proposed that the mixing and burning of fuel and oxidizer either in the wake formed by the oxidizer-rich gas stream behind the fuel droplets or in the shear layer between adjacent fuel-rich and oxidizer-rich streams could provide the energy feedback necessary to drive high frequency oscillations in the combustion chamber.[8,9] Interactions of acoustic fields as well as finite amplitude oscillations with boundary layers on flat plates and in pipes have been previously reported in the literature.[10,11,12] In those studies it has been shown that the interaction of the amplified disturbances with the mean flow field may lead to earlier transition to turbulence and increased rates of heat transfer.

In the present investigation, the effect of finite amplitude periodic oscillations, imposed at the boundaries of axisymmetric jet diffusion flames, has been studied both experimentally and theoretically. It is found that once an external disturbance is amplified in a flame, a reduction of the mean flame length and flattening of the mean temperature distributions takes place. A similar type of interaction of external oscillatory motion with cold jets has been reported as well.[13]

EXPERIMENTAL APPARATUS AND PROCEDURE

A choked stream of natural grade propane is exhausted as an axisymmetric jet of 1/2" diameter into a glass chamber (10" diameter) open at one end and is ignited by a torch. A uniform velocity distribution of about 3 ft/sec is established at the burner outlet. An oscillating air stream flowing at a a mean velocity of 1 ft/sec around the propane jet is introduced into the 10-inch diameter chamber via a system which consists of a needle valve mounted in parallel with a ball valve

rotated by a geared down variable speed motor. The frequency of oscillations is controlled by the motor speed while the amplitude is varied by altering the relative amounts of air passing through the needle-ball valve system.

Measurements of temperature distributions in the oscillating flames have been made employing a 0.003-inch diameter Pt-Pt 10% Rh bare thermocouple. The readings were corrected for radiation losses. Total and static pressure measurements were made with the aid of a pitot tube and a sensitive low pressure variable reluctance transducer. Radial and axial traverses of the oscillating flames were conducted at four frequencies (f = 2, 6.25, 15, 25 Hz) and two different amplitudes of the external flow oscillations as well as in steady state. A "point by point" measurement at a constant spacing of 1/4 inch between points, have been taken as well. The empirical data was recorded on tapes, and reduced by a high speed computer using an A/D converter. Average as well as rms values of the fluctuating pressures, velocities and temperatures were calculated at various points.

Velocity measurements in the investigated flames were made using a heat flux hot-wire probe. The heat flux probe sensor consisted of a nitrogen cooled quartz tube (0.006-inch diameter and 0.05-inch long) coated by a thin platinum film. The probe, which is available commercially, was calibrated in a hot nitrogen wind tunnel over a range of Nusselt and Reynolds numbers of 1-10 (based on the sensor diameter).

EMPIRICAL RESULTS

The effects of the external unsteady motion on the mean structure of the flame is shown in Figs. 3 and 4. The direct photographs (Fig. 3) show a shortening and a corresponding widening of the oscillating flame as compared to steady state. The largest interaction of the external flow with the flame field takes place (for the 1/2" burner) at a frequency of 14-20 Hz. At a lower or much higher frequency no significant changes of

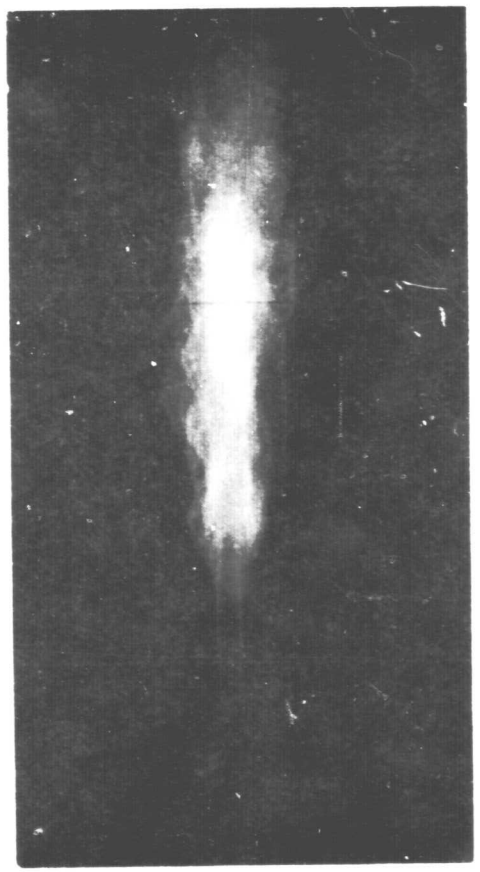

Steady-state flame

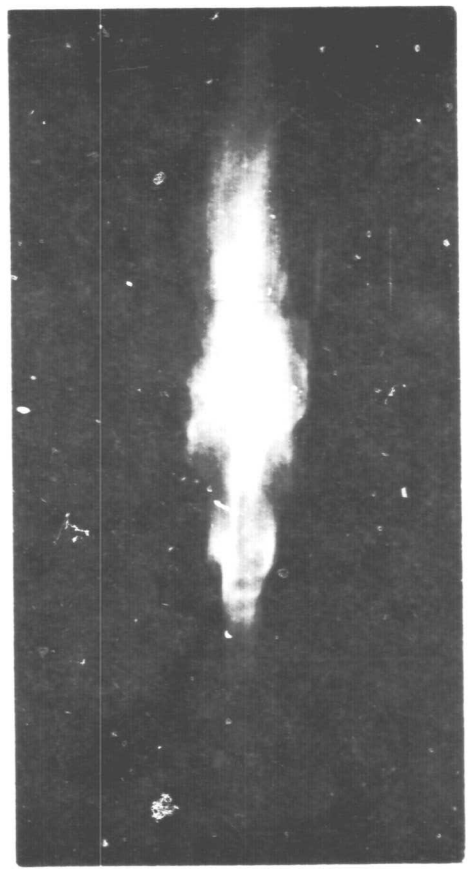

Oscillating flame
f = 15Hz Amp = 25 %

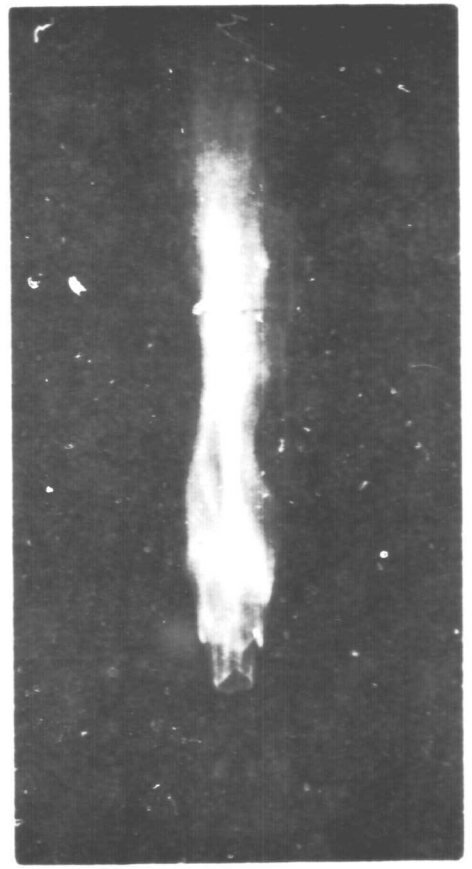

Oscillating flame
f = 15Hz Amp = 50%

Direct photographs of oscillating flames
($\frac{1}{2}$" Burner)

Figure 3

Steady-state flame

Oscillating flame
f = 15 Hz Amp = 25%

Oscillating flame
f = 15 Hz Amp = 50%

Shadowgraphs of oscillating flames
($\frac{1}{2}$" Burner)

Figure 4a

Oscillating flame
f = 44 Hz Amp = 25 %

Oscillating flame
f = 44 Hz Amp = 50%

Shadowgraphs of oscillating flames
($\frac{1}{2}$"Burner)

Figure 4b

the flames are observed. Shadowgraph pictures shown in Fig.4 suggest that the external unsteady flow interacted with the flame in the laminar flow region close to the burner outlet. At 15 cps the oscillations cause a symmetric widening of the flame field and a severe disruption of the potential core region (which consists mainly of gaseous fuel) at large amplitudes. Mixing is thus enhanced and the burning rates at the region of interaction are most likely increased. The effects shown diminish with increasing frequency as is evident from the pictures taken at 44 Hz.

A radial distribution of temperature at a distance of 6 diameters downstream of the burner outlet is shown in Fig. 5 for a frequency of 15 Hz. The amplitude effects seem to mainly result in the flattening of the steady-state temperature profiles and an increase in the spread of the thermal layer. Also, due to increased mixing, the maximum flame temperature drops down and is maintained at relatively low values compared to the steady state. The increased mixing and intensification of the burning due to the external oscillations is observed also in Fig. 6, which shows the variation of the temperature on the flame axis. It is seen that higher temperature and shorter potential core regions are associated with increased amplitudes of the external oscillations. The location of the maximum temperature in the flame may be representative of a flame "front" as plotted in Fig. 7. The figure shows that the mean length of the largest amplitude oscillatory flame is the smallest. The temperature fluctuations may be described by the root-mean-square values of the instantaneous oscillations as plotted in Fig. 8 (for a frequency of 15 Hz). One immediately notes that the radial distribution of the rms values of the temperature fluctuations follow the general shape of the mean temperature distribution, yet the location of the maximum values do not coincide with the mean temperature maximums.

When plotting the maximum rms value along the axis of the flame (Fig. 9) it is seen that an amplification of the

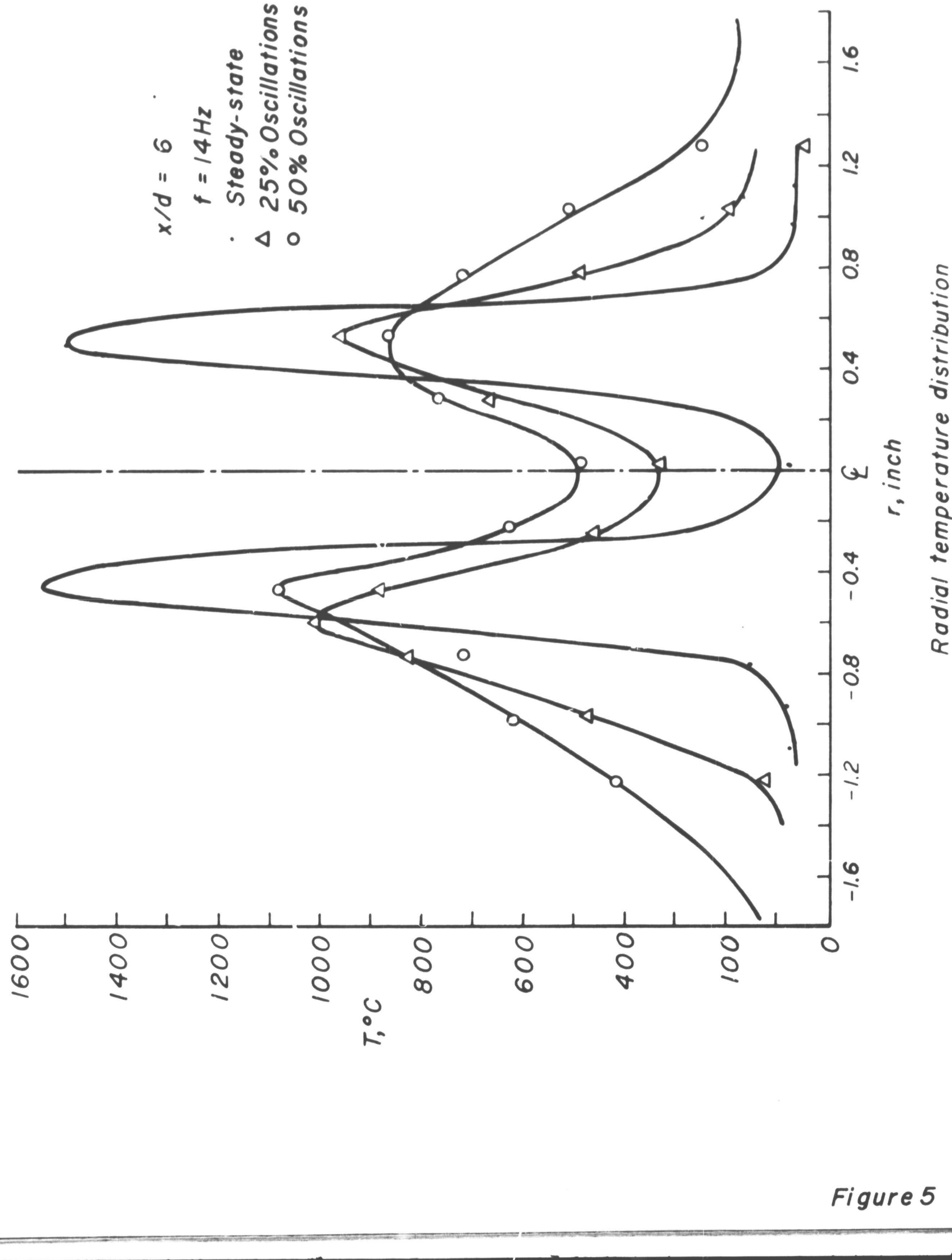

Radial temperature distribution

Figure 5

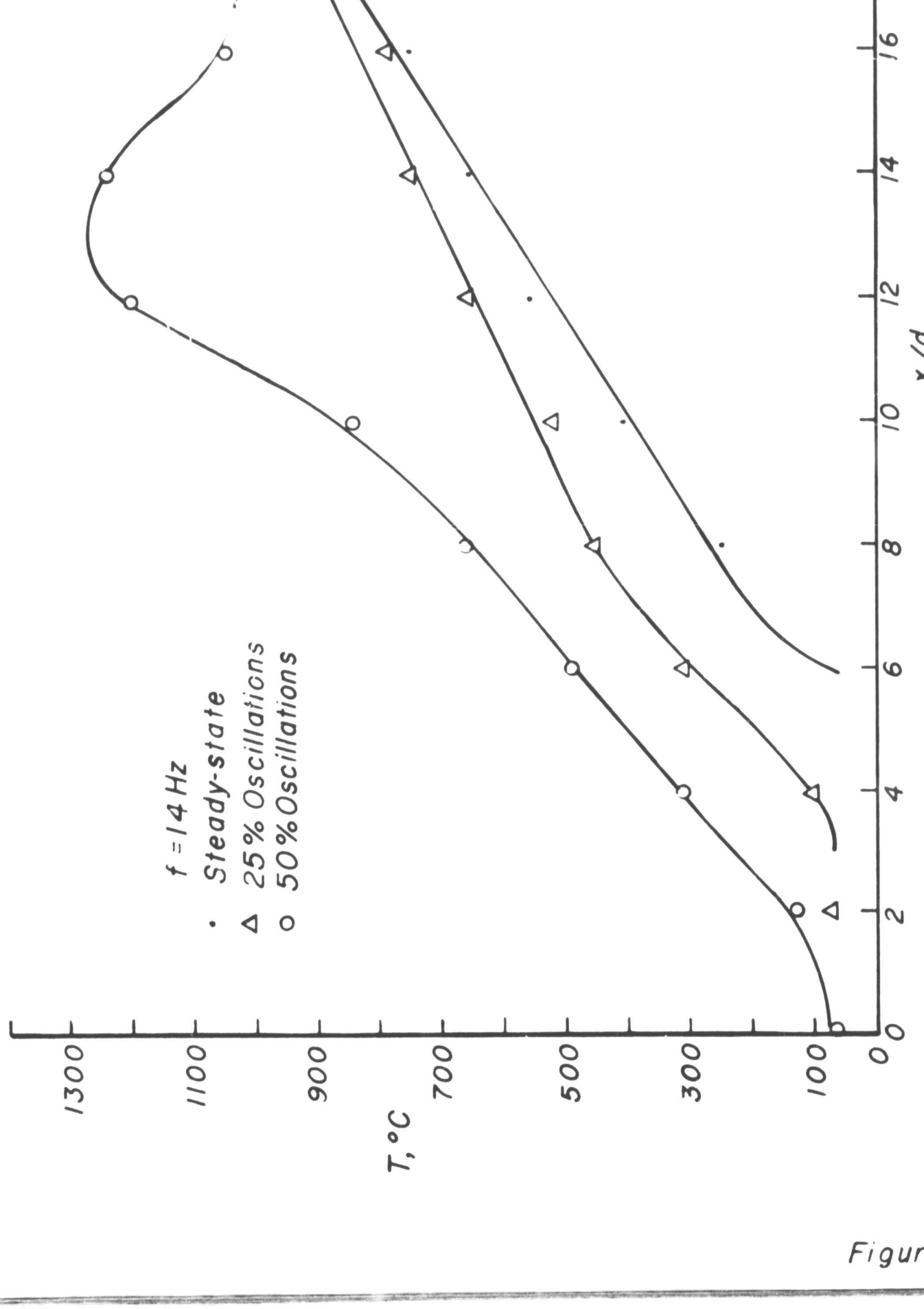

Variation of temperature on the flame axis

Figure 6

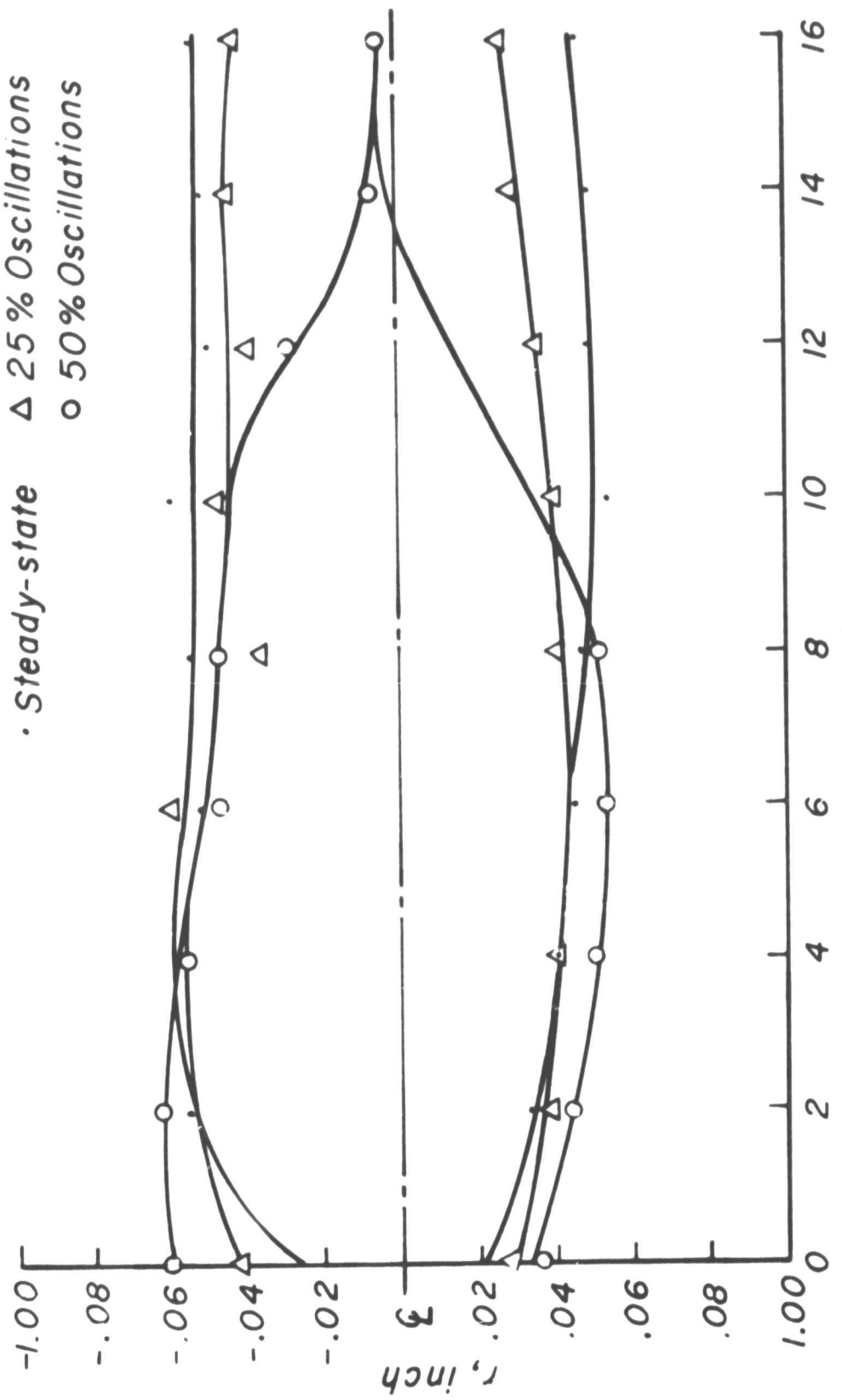
f = 14 Hz
Δ 25 % Oscillations
o 50 % Oscillations
· Steady-state
-1.00
-.08
-.06
-.04
-.02
r, inch
.02
.04
.06
.08
1.00
0
2
4
6
8
10
12
14
16
x/d
Flame front lines
(Contour of temp. max.)

Figure 7

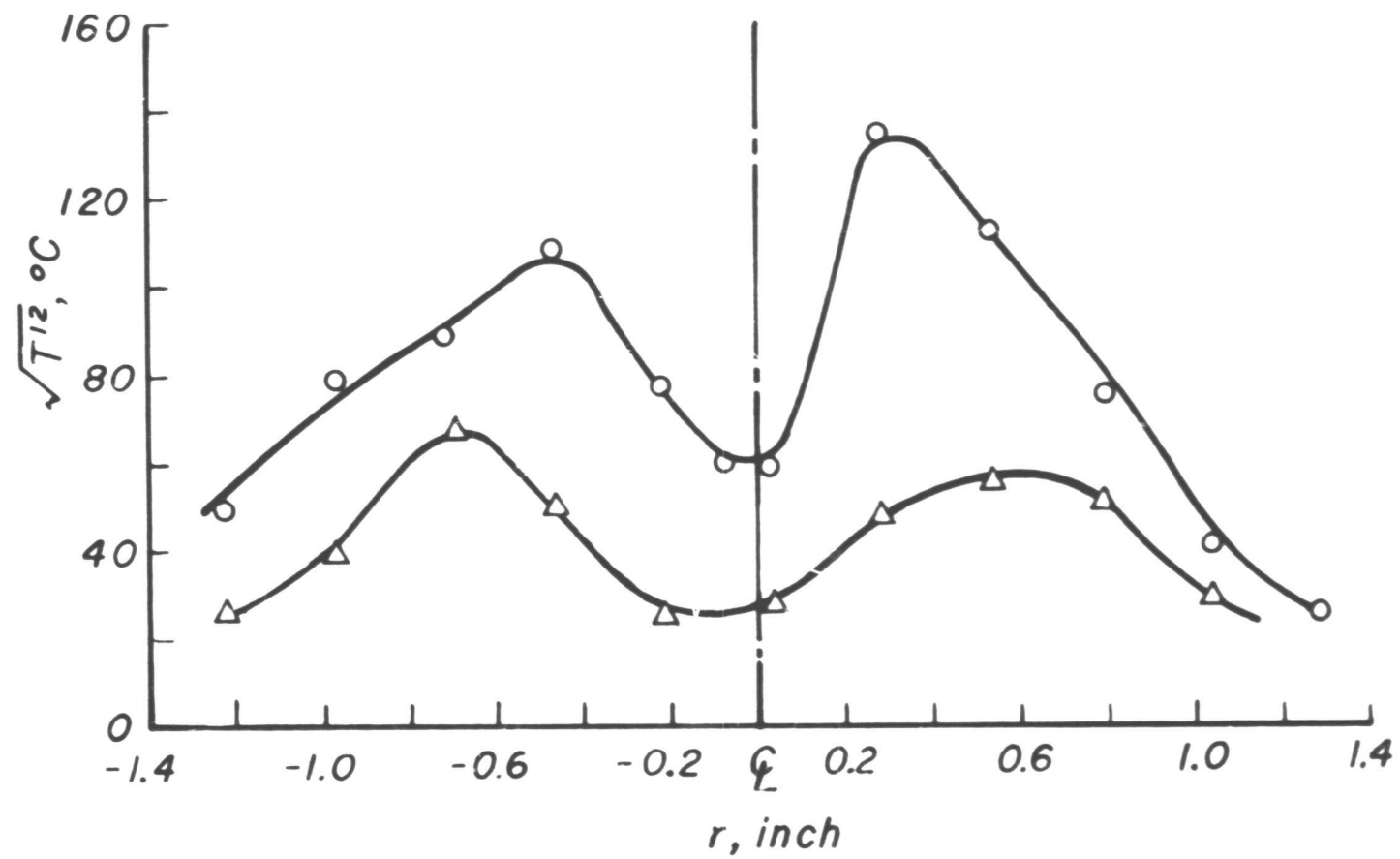

Radial distribution of, $\sqrt{T'^2}$

Figure 8

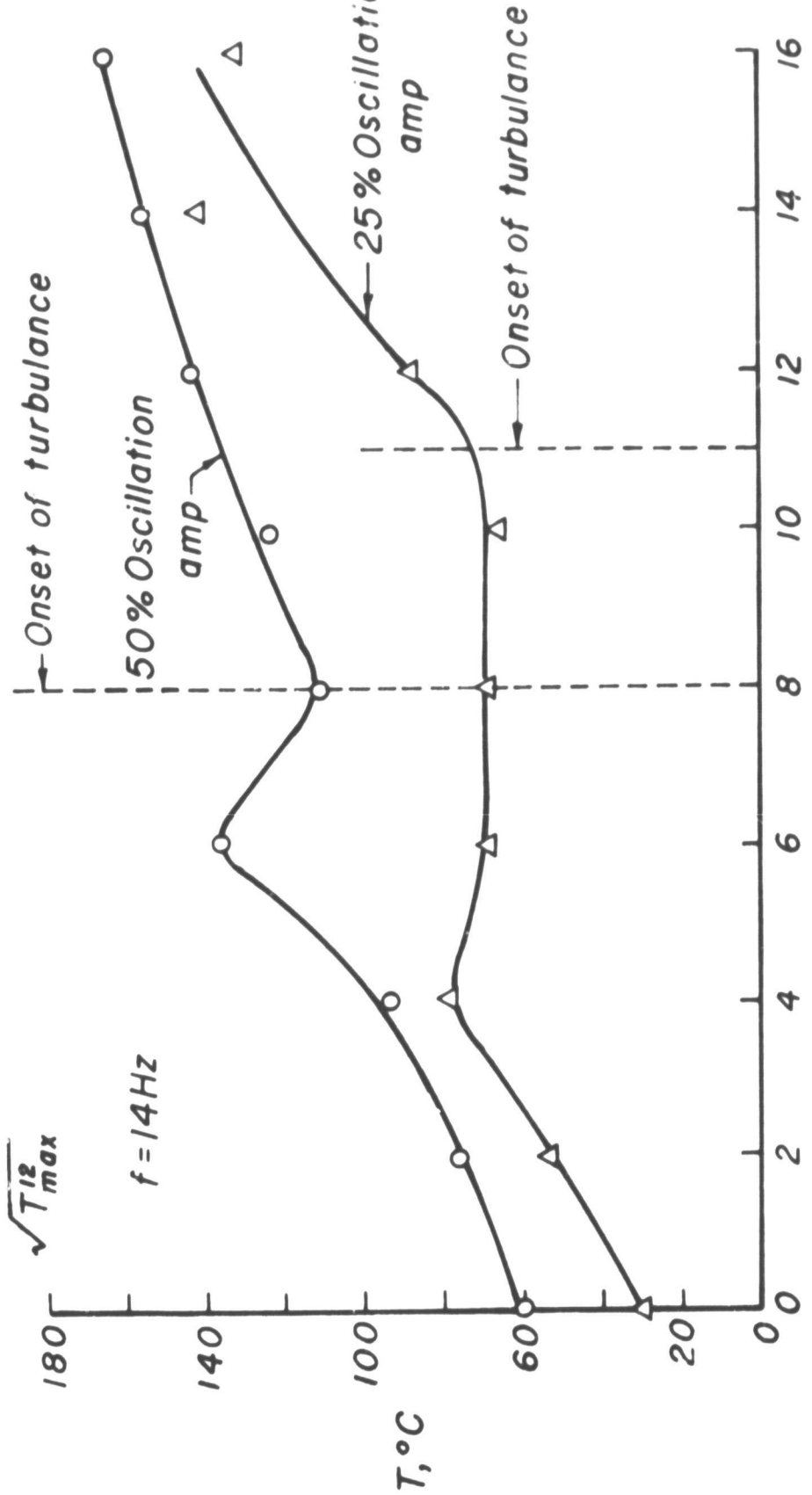

Variation of maximum value of RMS temperature fluctuation along the flame axis

Figure 9

temperature oscillation in the flame occurs between 4 and 6 diameters downstream of the burner outlet. A decay of the rms values followed by an increase of amplitude due to turbulence takes place further downstream. The plot also suggests that the onset of turbulence in flames may be enhanced by large amplitude external oscillations.

In the present experiments no amplification of static pressure oscillation in the 10-inch diameter chamber were detected. The amplitude of pressure oscillations remained essentially uniform across the chamber and decayed somewhat in the axial direction.

THEORETICAL STUDY AND RESULTS

The theoretical study of oscillatory free diffusion flames was divided into a study of the mixing region far from the burner outlet and an examination of the potential core flow field region. In the present report theoretical results describing the interaction of the far field of an axisymmetric free diffusion flame with external velocity oscillations are given and discussed in the limit of high frequency. Assuming that the flow field is axisymmetric, that body forces and radiation effects are negligible, and that chemical reactions occur only at a flame surface, the time-dependent boundary layer conservation equations are written for Lewis number unity and a constant heat capacity of the mixture.

Employing the Howarth transformation and assuming that the external velocity far away from the flame is given by

$$U_1 = \bar{U}_r(1 + \epsilon e^{i\omega t}) \qquad (1)$$

where

$$\bar{U}_r = \bar{U}_o - \bar{U}_\infty$$

and the conservation equations are written as[14]

$$\frac{\partial(\hat{u}R)}{\partial \xi} + \frac{\partial(\hat{v}R)}{\partial R} = 0 \tag{2a}$$

$$S\frac{\partial \hat{u}}{\partial \tau} + \hat{u}\frac{\partial \hat{u}}{\partial \xi} + \hat{v}\frac{\partial \hat{u}}{\partial R} = S\,h\frac{dU_1}{d\tau} + \frac{1/Re}{R}\frac{\partial}{\partial R}\left[\mu\rho\left(\frac{r}{R}\right)^2 R\frac{\partial \hat{u}}{\partial R}\right] \tag{2b}$$

$$S\frac{\partial \beta}{\partial \tau} + \hat{u}\frac{\partial \beta}{\partial \xi} + \hat{v}\frac{\partial \beta}{\partial R} = -\frac{S\bar{\beta}_r}{q_o}(\gamma - 1)M_r^2\, h(\hat{u} - U_1)\frac{dU_1}{d\tau} + \frac{1/Re}{R}\frac{\partial}{\partial R}\left[\frac{\mu\rho}{Pr}\left(\frac{r}{R}\right)^2 R\frac{\partial \beta}{\partial R}\right] \tag{2c}$$

$$S\frac{\partial \Gamma_i}{\partial \tau} + \hat{u}\frac{\partial \Gamma_i}{\partial \xi} + \hat{v}\frac{\partial \Gamma_i}{\partial R} = \frac{1/Re}{R}\frac{\partial}{\partial R}\left[\frac{\mu\rho}{Pr}\left(\frac{r}{R}\right)^2 R\frac{\partial \Gamma_i}{\partial R}\right] \tag{2d}$$

where $\hat{u}$ is a dimensionless axial component of the velocity $\hat{v}$ is a modified radial velocity and β and Γ_i are the Shvaab-Zeldovich enthalpy and concentration of species i variables. $S = \frac{\omega r_e}{\bar{U}_r}$; $Re = \frac{\bar{U}_r r_o}{\nu_\infty}$ and $M_r = \frac{\bar{U}_r}{c_\infty}$. For more details see Ref. 14.

Assuming that the dependent transformed variables may be separated into a mean part which is not a function of time plus a time-dependent fluctuation and introducing those expressions into Eqs. (2a)-(2d) one obtains a time-dependent nonlinear set of equations which includes mean as well as non-linear time dependent variations from that mean. For small amplitudes of external flow oscillations ($\epsilon << 1$), the mean values in those equations may be identified with the steady-state variables. Also, in that limit a linear set of time-dependent equations for the fluctuations may be derived. The solutions of the steady-state equations in the far mixing region may be expressed in the form:

$$\frac{\bar{U} - \bar{U}_\infty}{\bar{U}_o - \bar{U}_\infty} = \frac{c_1}{2\eta_W}\exp\left(-\frac{R^2}{4\eta_W}\right) \tag{3a}$$

$$\frac{\bar{\beta} - \bar{\beta}_\infty}{\bar{\beta}_o - \bar{\beta}_\infty} = \frac{c_2}{2\eta_M}\exp\left(-\frac{R^2}{4\eta_M}\right) \quad ; \quad \frac{\bar{\Gamma}_i - \bar{\Gamma}_{i\,\infty}}{\bar{\Gamma}_{i\,o} - \bar{\Gamma}_{i\,\infty}} = \frac{c_3}{2\eta_M}\exp\left(-\frac{R^2}{4\eta_M}\right) \tag{3b,c}$$

where subscript o denotes the dependent variables values at the surface of the moving sphere (in case of a wake) or at the outlet of a jet (in case of a jet) and subscript ∞ denotes values far from the flame in the oscillating surroundings.

$$\eta_W = \int_o^\xi \bar{\mu}(\xi)\, d\xi \quad ; \quad \eta_M = \int_o^\xi \frac{\bar{\mu}(\xi)}{Pr(\xi)}\, d\xi$$

Employing the flame surface concept one may derive from Eqs. (3a-3c) the solutions for temperature and species i distribution in the flame when a one-step chemical reaction takes place at that surface only.

The solutions of the linear set of equations for time-dependent fluctuations in the limit of high frequency may be given as:

$$\frac{u'}{\bar{U}_o - \bar{U}_\infty} = \left\{ \bar{h} - \bar{\mu}(\xi)\, \alpha^2 \left(\frac{\partial \bar{h}}{\partial \eta_M} + \bar{h} \frac{\partial \bar{W}}{\partial \eta_W} \right) + O(\alpha^4) \right\} \epsilon\, e^{i\omega t} \qquad (4a)$$

$$\frac{\beta'}{\bar{\beta}_o - \bar{\beta}_\infty} = \left\{ - \frac{\bar{\mu}(\xi)}{Pr(\xi)}\, \alpha^2 \left(\frac{\partial \bar{\beta}}{\partial \eta_M}\, h \right) + O(\alpha^4) \right\} \epsilon\, e^{i\omega t} \qquad (4b)$$

$$\frac{\Gamma_i'}{\bar{\Gamma}_{i\,o} - \bar{\Gamma}_{i\,\infty}} = \left\{ - \frac{\bar{\mu}(\xi)}{Pr(\xi)}\, \alpha^2 \left(\frac{\partial \bar{\Gamma}_i}{\partial \eta_M}\, \bar{h} \right) + O(\alpha^4) \right\} \epsilon\, e^{i\omega t} \qquad (4c)$$

where $\alpha^2 = \frac{1}{Re\ S}$ and $\bar{W} = \bar{U} - \bar{U}_\infty$. The linear fluctuations of fuel and temperature are thus inversely proportional to and therefore disappear at infinite frequency. The effects of the linear fluctuation on the steady-state flame location is shown in Fig. 10 where the maximum deviation of the flame front from its steady-state value is depicted. For propane gas burning stoichiometrically in air the K values of .1 and .4 correspond to ϵ/Re S = .005 and 0.02 respectively. When the

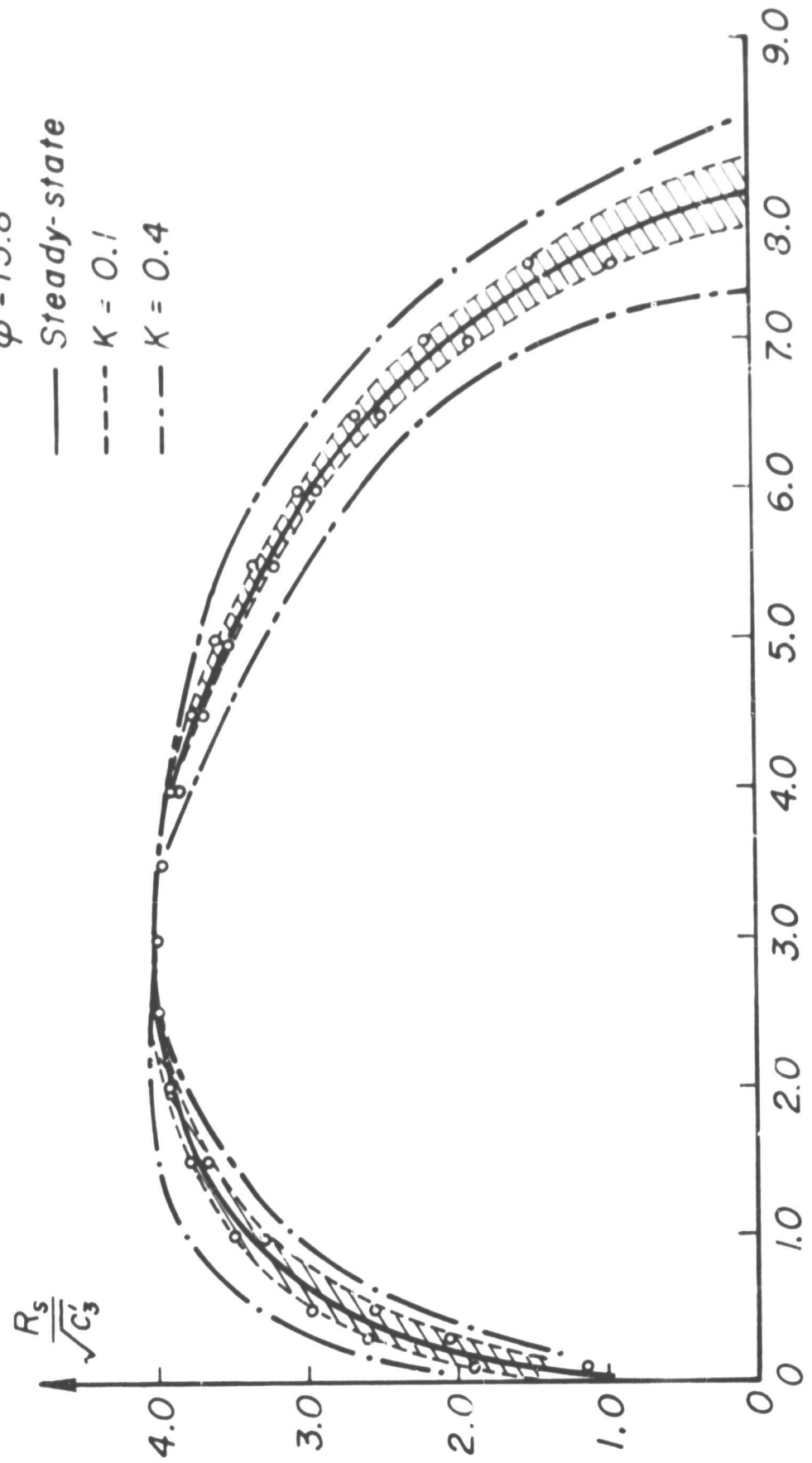

Linear effects of oscillation on flame front location

Figure 10

amplitude of the external velocity oscillations ϵ is no longer small, the mean variables of the flow field can no longer be given by the steady-state solutions. Also, nonlinear terms become important and may not be neglected. Going back to the time-dependent nonlinear equations derived from Eqs. (2a)-(2d), an averaging of the equations over a long period of time is carried out and yields nonlinear equations for the mean variables similar to those obtained in the theory of turbulent flows. Integrating those equations in the radial direction from the axis of symmetry to infinity the following equations result:

$$\int_0^\infty \frac{\partial}{\partial \xi} \left[(\bar{\bar{U}} - \bar{\bar{U}}_\infty) + \bar{\bar{u}}'^2 \right] RdR = S \int_0^\infty \overline{\overline{h' \frac{dU_1}{d\tau}}} \, RdR \qquad (5a)$$

$$\int_0^\infty \frac{\partial}{\partial \xi} \left[(\bar{\bar{\beta}} - \bar{\bar{\beta}}_\infty) + \overline{\overline{u'\beta'}} \right] RdR = 0 \quad ; \quad \int_0^\infty \frac{\partial}{\partial \xi} \left[(\bar{\bar{\Gamma}}_i - \bar{\bar{\Gamma}}_{i\,\infty}) + \overline{\overline{u'\Gamma_i}} \right] RdR = 0 \qquad (5b,c)$$

$$\int_0^\infty \frac{\partial}{\partial \xi} \left[(\bar{\bar{U}} - \bar{\bar{U}}_\infty)^2/2 \right] RdR + \frac{\bar{\mu}(\xi)}{Re} \int_0^\infty \left(\frac{\partial \bar{\bar{U}}}{\partial \xi}\right)^2 RdR = 0 \qquad (5d)$$

where double bars denote "mean values". In Equations (5a)-(5d) none of the variables is known a priori. An assumption based on empirical evidence part of which is shown in Figs. 3-9 is made. We assume that the general shape of the mean variables and of the fluctuations when ϵ is no longer small is still similar to the shape of the steady-state and small oscillations in the flame. Scales of the distributions of the variables are the only quantities which are allowed to vary due to external oscillations. Thus one defines a velocity scale $\bar{U}(\epsilon) - \bar{U}_\infty$, enthalpy and mass concentration scales, and momentum and thermal layer thicknesses. Introducing the solutions found for the steady-state variables and the linear fluctuation expressed in terms of the unknown scales into Eqs. (5a)-(5d) four ordinary differential equations for the five unknown scales are obtained. One may also

add now a correlation between the momentum and thermal thicknesses (via the Prandtl number) thus obtaining a closed system of five ordinary differential equations for the five unknown scales. Numerical solutions of the set have been obtained up to $O(\alpha^2)$. Changes of the mean length of the flame due to the external oscillations are shown in Fig. 11. The theory predicts a shortening of the flame length with increased ϵ and an increase of the initial width b_o of the flame. This is in qualitative agreement with the empirical observations of Figs. 3 and 5.

Extension of the present theory to the case when the Mach number of the external flow is no longer negligible is currently under way. In that case the external flow velocity is expressed in the form $U_1 = \bar{U}_r[1 + \epsilon\, e^{i(t - \frac{MS}{M+1}\xi)}]$. Mach number effects are therefore introduced into the equations and numerical solutions are obtained.

CONCLUSIONS

External periodic disturbances interact with free diffusion flames over a range of frequencies. When such an interaction occurs the mean length of the flame is decreased with increasing amplitude of external oscillation, and a corresponding widening of the flow field follows.

As indicated in Fig. 9, the external oscillations increase mixing rates in the flame and may cause an early transition to turbulence which is manifested by a shortening of the potential core region of the flame.

The distributions of the temperature fluctuations in the flame are similar in shape to the mean temperature distribution. At the critical frequency those oscillations are amplified in the boundaries of the flame somewhat off the point point of mean temperature maximum. Amplification of the temperature oscillations in the flame may be a sign of increased instantaneous burning rates yet definite conclusions regarding

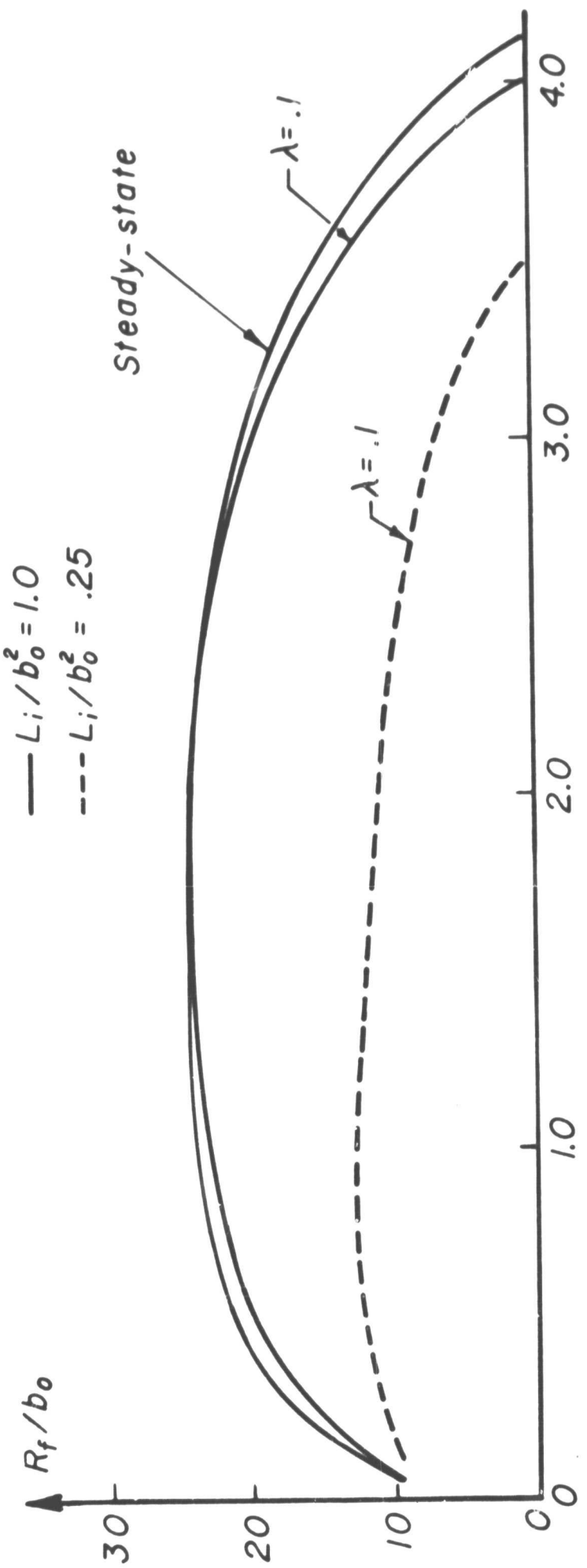

Mean changes of flame front line

Figure 11

that point must be deferred until all the measurements are completed.

The theoretical analysis carried out for high frequency is in good qualitative agreement with the empirical data. This may be a justification of cur assumption regarding the relation of the variables of the flow field when ϵ is small to the same variables when ϵ is significant.

VII. THEORETICAL INVESTIGATIONS OF TRANSVERSE MODE COMBUSTION INSTABILITY

INTRODUCTION

It has long been recognized that improved theoretical analysis of the combustion instability problem is necessary if stable operation is to be insured. This research is seeking a quantitative understanding of the combustion processes, which occur in the conversion of injected propellants to burned combustion gases, and the damping processes in the combustion chamber. The parameters n and τ in the sensitive time lag theory, although successful in predicting stability boundaries, must still be related to the physicochemical process involved. Also, the theory must take into account triggering phenomena. The present theory attempts to achieve these aims with a droplet evaporation model to calculate combustion source terms and to relate the instability conditions to the mass/energy release in the chamber.

The gas dynamic equations for the annular chamber have been developed. This chamber was selected because it affords considerable simplification of the theory as compared to a cylindrical combustion chamber and also the annular chamber results will be useful for future combustion chamber configurations. The fuel vaporization is generally acknowledged to be the rate limiting process in the conversion of injected propellants into burnt gases. Consequently a quasi-steady droplet vaporization model, as developed by Priem and Heidmann[15], is used to calculate the mass/energy sources for the gas dynamic equations. The equations are solved by the technique of expansion in powers of a small parameter, related to the perturbation amplitude.

In the process of carrying out this research several aspects of the problem have received considerable attention.

One is the mathematical techniques necessary to attack certain aspects of the nonlinear problem. Such a technique is the coordinate perturbation technique. These studies are described next.

THE COORDINATE PERTURBATION TECHNIQUE

The coordinate perturbation technique has been used to obtain uniformly valid solutions to certain nonlinear equations which have importance to the study of combustion instability. This approach is also termed the coordinate stretching (or straining) technique, or the PLK (Poincaré-Lighthill-Kuo) method. Despite the importance of the technique, applications have been limited because of the intricacies associated with the usual way of applying it, which involves transforming the equations to new, perturbed, independent variables. The trouble comes from the fact that the transformed equations become almost hopelessly complicated and confusing with an increasing number of variables, order of the equations, and order of the approximation. In a paper authored by L. Crocco, which will be available shortly, these points are clarified. This paper shows how the application of the method can be drastically simplified by avoiding the transformation of the equations and working directly on the nonuniformly* valid solution (resulting from direct expansion) to obtain the uniformly valid expansion.

As an illustration, the procedure is applied to the ordinary differential equation of the oscillation with a cubic restoring force, and to two problems governed by partial differential equations. In the first of these problems the complete flow field around a supersonic two-dimensional wing is determined up to third order, including the shock shape. In the second problem, which applies to combustion instability, the study of nonlinear oscillations

---

* Areas exist in the field of interest where the solution is in error due to mathematical difficulties.

following an initial disturbance in a closed pipe is conducted with two different types of boundary conditions. With two closed ends one gets waves that are slowly distorted until a shock appears, after which the waves decay. With one closed end and a harmonically driven piston at the other end, oscillations are produced which tend to a periodic solution containing or not containing shocks depending on the piston frequency. The corresponding solution by Chester is discussed in the forthcoming paper.

One interesting observation is that in both problems it is found that the resulting solutions are not only uniformly valid, but also substantially simpler in form than the nonuniformly valid expansions. Moreover, in both problems one is forced into adding to the coordinate perturbation technique the multiple scale technique. The latter is required to take into account other factors associated with wave motion that would be obscured if the scale was not altered.

VIII. UNSTEADY DROPLET BURNING: THERMAL RESPONSE OF THE CONDENSED PHASE FUEL ADJACENT TO A REACTING GASEOUS BOUNDARY LAYER

INTRODUCTION

An investigation was undertaken to determine the responses of a burning droplet in a convective stream where the external flow has a longitudinal oscillation. The purpose is to try to isolate the physical mechanism wnich leads to combustion instability in liquid propellant rockets. The problem is the same as the one treated by Priem and Heidmann[15], Strahle[16] and Williams[17]. However, the physical mechanism under investigation is different. Instead of assuming the droplet temperature to be uniform and/or constant, it is assumed that there can be a nonuniform temperature distribution inside the droplet.

The investigation of Wise and Ablow[18] showed that during steady-state burning the temperature distribution in the liquid droplet depends on the dimensionless ratio of burning rate coefficient to thermal diffusivity of the liquid. For the case of rocket combustion, the burning is vigorous and this ratio is large. In this case, significant nonuniform temperature distribution persists throughout the first half-life-time of the droplet. As a consequence, when the pressure oscillates, an unsteady heat transfer process will occur inside the droplet. An estimate of this heat diffusion time shows that it is of the same order as the characteristic time of rocket motor oscillations. Therefore it is felt the unsteady heat transfer inside the droplet is important and should be taken into account.

For typical droplet size and relative gas velocity, the gas residence time in the boundary layer is an order of magnitude smaller than the condensed phase diffusion time or the period of oscillation. Thus the gas phase can be

treated in a quasi-steady-state manner. The problem here, in contrast to Strahle's, has a nonsteady condensed phase but a quasi-steady gas phase. The "time lag" that is sought is related to the thermal inertia of the liquid.

As in the analysis of Strahle, various points on the droplet surface can be simulated by the wedge flow of different angles of attack. The results of the flat plate analysis, which is a wedge with zero angle, are presented here. The extension to the cases of non-zero angle wedge is readily made using the present formulation. The flat plate case nevertheless is a representative point around the droplet surface and its results therefore give good indication whether amplification is possible or not under the present formulation.

DISCUSSION

The analysis will not be covered here, but emphasis is placed on the results and discussion.

The base case parameters are taken to be droplet center temperature: $T_o/\bar{T}_e = 0.2$, latent heat of the fuel $\mathcal{L}/c_p\bar{T}_e = 0.35$, the heat of combustion $q/c_p\bar{T}_e = 4.0$, the steady-state pressure $\bar{p}/h = 3\ e^{-4}$, and the external oxidizer mass fraction $\bar{Y}_{oe} = 0.6$.

The wave is assumed to be a fundamental mode standing wave (only for the demonstrative purpose), then $p'/\bar{p} = \cos\pi z$ and $u_e'/\bar{c} = -i/\gamma \sin\pi z$. Depending on whether the droplet is accelerated or decelerated by the gas, the relative velocity has the opposite or the same sign as u_e', which is defined positive in the positive z direction. Therefore, $u_e'/\bar{u}_e = \mp (i/\gamma M_{rel})\sin z$, with a minus sign for accelerated droplet while the positive sign signifies a decelerated droplet. By specifying the position of the droplet (z) and the position of zero relative velocity, the burning rate response $\mathcal{R}$ can be calculated. Crocco has shown[8] that in

order to have longitudinal instability, the quantity

$$G = \int_o^1 \frac{dV_1}{dz} \mathcal{R}_R \cos \pi z dz \qquad (1)$$

must be large enough. For the case of very short nozzle and negligible drag and convective losses, G must be larger than one half to have instability. For illustrative purposes, it can be assumed that all the droplets evaporate instantaneously at one quarter of the chamber length from the injector head ($z = 1/4$), and are accelerated by the gas. Then $G = \mathcal{R}_R \cos \pi/4$. Taking $\gamma = 1.25$, $M_{rel} = .02$ and the base case parameters, it is seen from Fig. 12 that G has a peak centering about $\omega = 1$ and its magnitude is greater than one half. Therefore, under favorable conditions, instability is possible using the present model. The peak of G will increase if M_{rel} decreases, but is a singular region for this study, since boundary layer does not exist. Furthermore, the distributed combustion will decrease the G value.

Assuming the droplets are injected into the combustion chamber with a finite velocity in axial direction, it can be shown that for distributed combustion two cases can be distinguished. In Case 1, the point of zero gas-droplet relative velocity is ahead of the pressure nodal point. In this case, three regions can be divided. In the region between these two points, both the pressure and velocity contributions to G are positive. In the region close to the injector, the pressure contribution is positive but the velocity contribution is negative so they tend to cancel each other. In the region close to the nozzle the pressure contribution is negative, the velocity contribution is also negative but is in general very small because the droplets are heated up and the temperature inside the condensed phase tends to be uniform (this temperature uniformity effect will be discussed later). In Case 2, the point of zero relative velocity is behind the pressure node. In the region between these two points, the

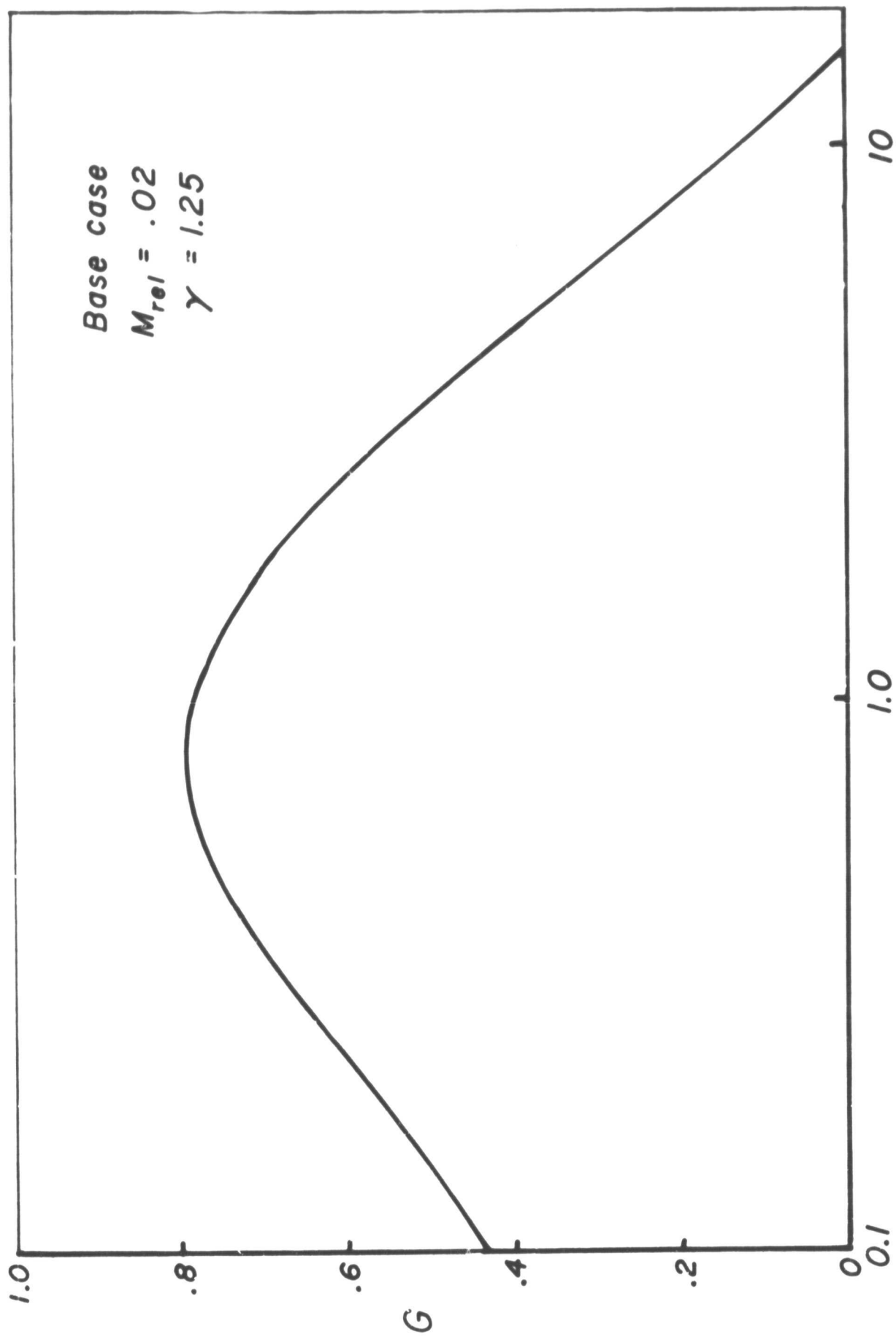

In phase energy release vs frequency

Figure 12

velocity contribution is positive although the pressure gives negative contribution. The two other regions are the same as in Case 1. Therefore, it is seen that for distributed combustion, the most favorable situation for instability to occur is Case 1 with most burning occurring in the intermediate region.

The pressure-sensitive part $(\dot{m}'/\bar{\dot{m}})/(p'/\bar{p})$ is the response at the pressure antinode for a standing wave. The velocity-sensitive part $(\dot{m}'/\bar{\dot{m}})/(u_e'/\bar{u}_e)$ is the response at the velocity antinode. To obtain $\mathcal{R}_R$ from these two functions, we have

$$\mathcal{R}_R = \left[\frac{\dot{m}'/\bar{\dot{m}}}{p'/\bar{p}}\right]_R \pm \frac{1}{\gamma M_{rel}} \frac{\sin\pi z}{\cos\pi z} \left[\frac{\dot{m}'/\bar{\dot{m}}}{u_e'/\bar{u}_e}\right]_I \qquad (2)$$

again + , indicates an accelerating droplet and - a decelerating droplet.

In calculating $\mathcal{R}_R$, the contribution from the velocity-sensitive part is amplified by the factor $1/\gamma M_{rel}$. Since $M_{rel} << 1$, it is significant although the values of $(\dot{m}'/\bar{\dot{m}})/(u_e'/\bar{u}_e)$ are much smaller than that of $(\dot{m}'/\bar{\dot{m}})/(p'/\bar{p})$.

Figs. 13-15 show some of the results. The imaginary part of the velocity sensitive responses in general have a peak around $\omega = 1$. From Fig. 13, it is seen that this response increases with smaller external oxidizer mass fraction, lower combustion heat and larger latent heat. The pressure-sensitive responses do not have any peak. For low frequencies, they are nearly quasi-steady, for higher frequencies, they decrease monotonically. From Fig. 14, decreasing the external temperature $(\bar{T}_e)$, increases both the velocity and pressure sensitive responses, and by lowering the steady-state pressure, the velocity-sensitive response is decreased but the pressure-sensitive response is increased.

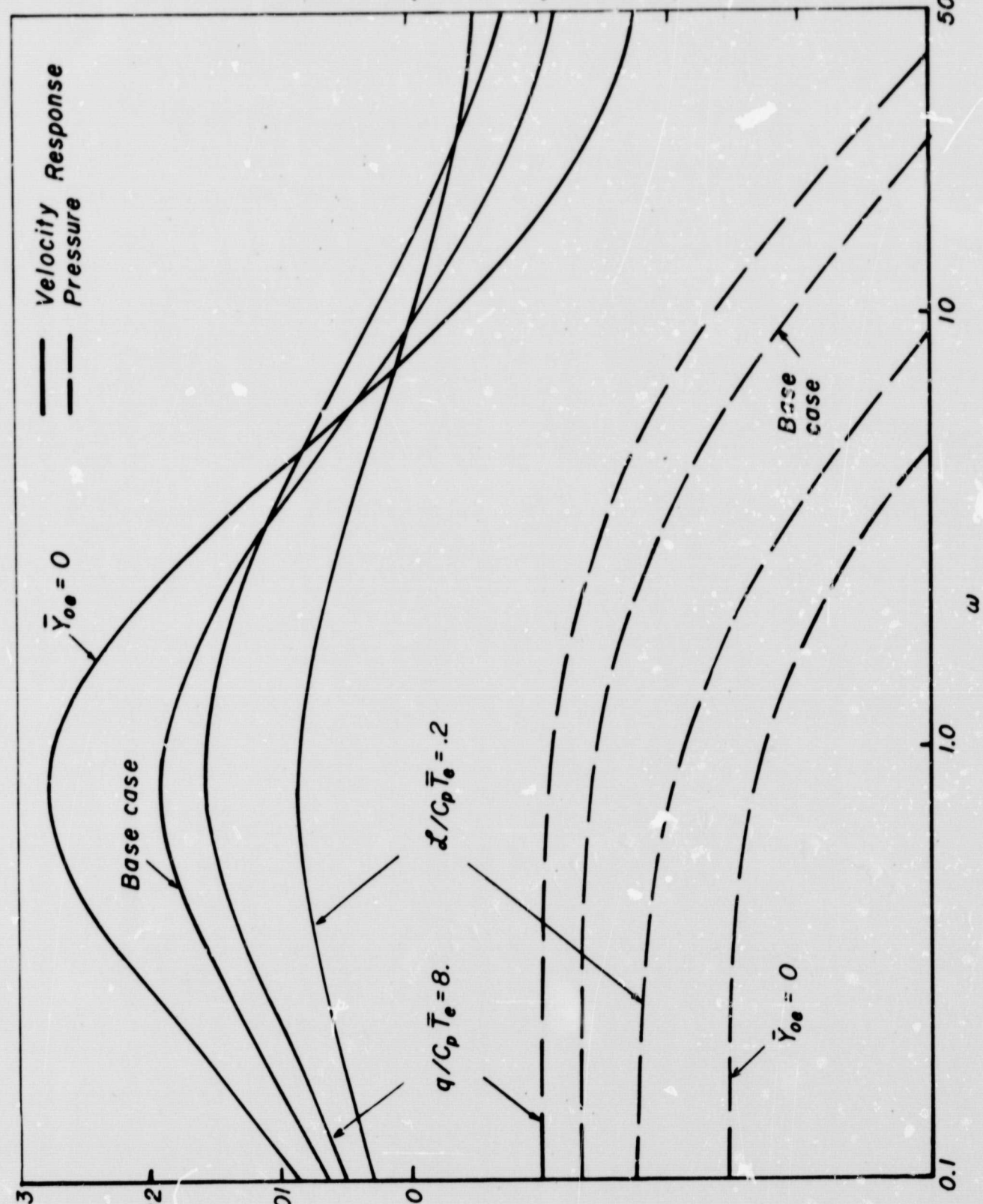

Parametric studies regarding response functions

Figure 13

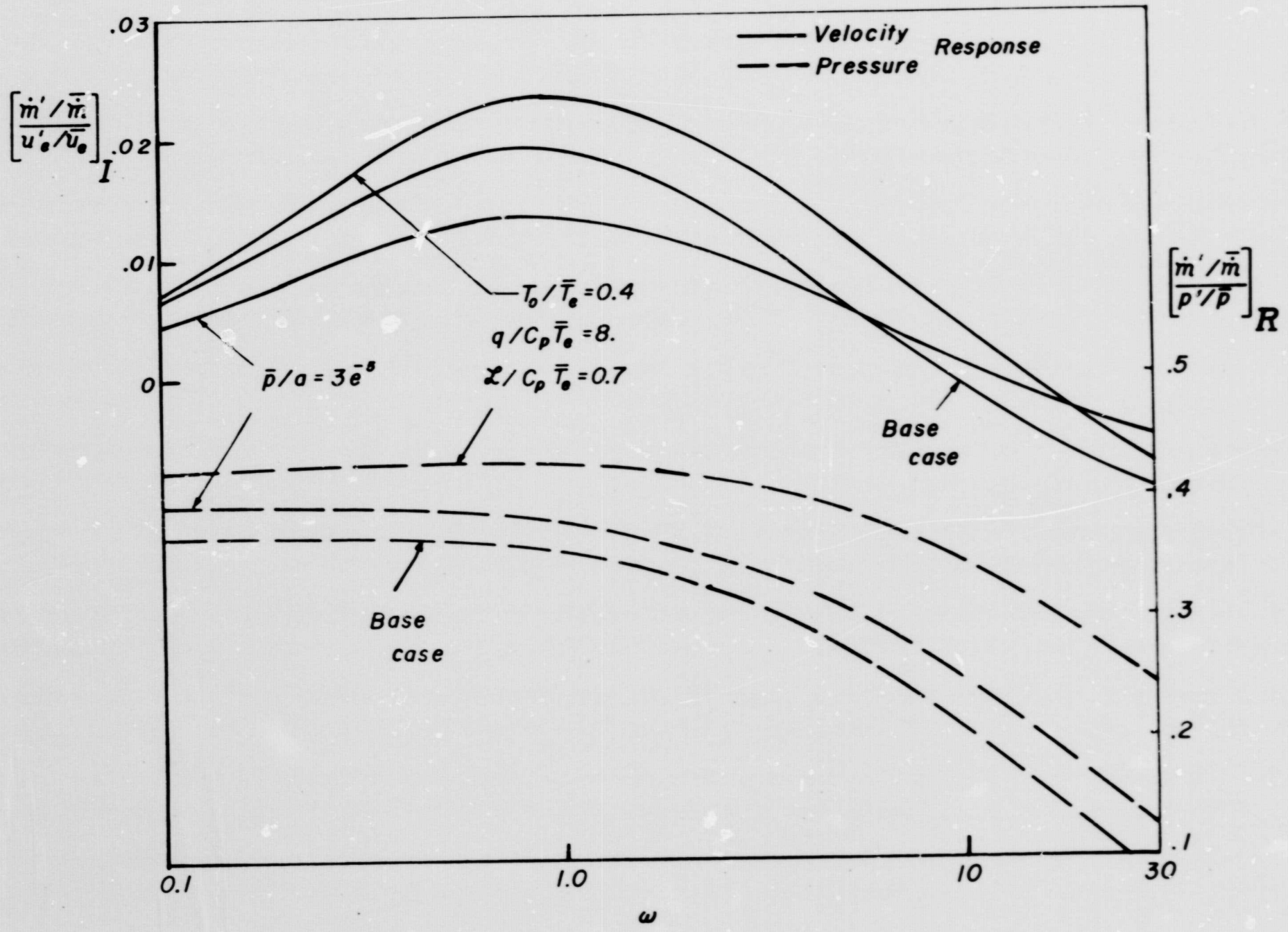

Figure 14

Parametric studies regarding response functions

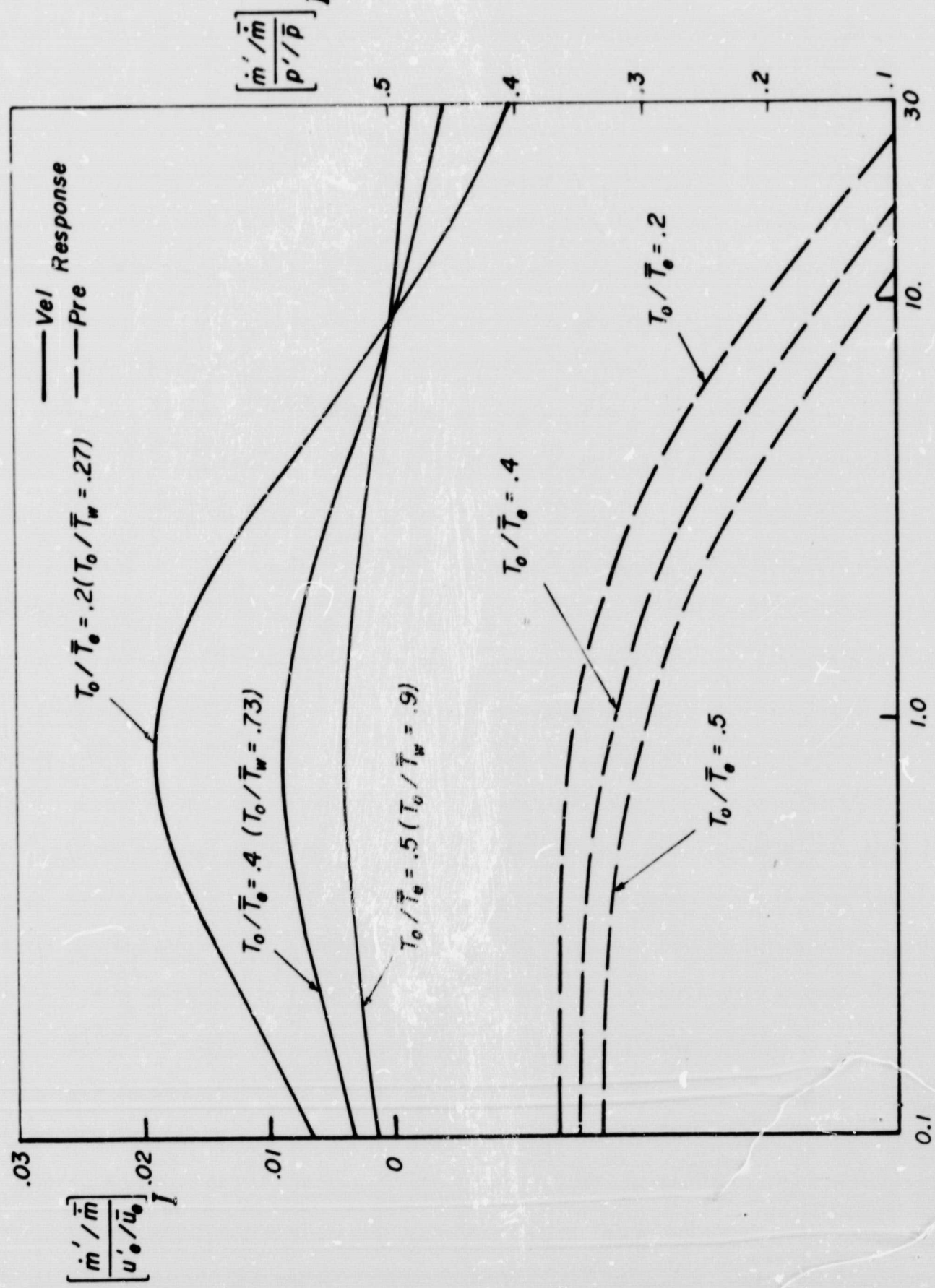

Influence of condensed phase temperature nonuniformity of response function

Figure 15

Fig. 15 shows the importance of the temperature nonuniformity in the condensed phase. While the pressure-sensitive responses do not change much as $T_o/\bar{T}_w$ varies, the velocity-sensitive part changes drastically. As the center temperature of the droplet approaches the surface temperature, the velocity response diminishes. As a consequence, the peaking and the instability are not possible. This is a further indication that the thermal lag in the droplet can be an important mechanism in driving the liquid rocket into instability.

IX. CHEMICAL KINETIC INFLUENCES IN LIQUID PROPELLANT ROCKET COMBUSTION INSTABILITY

INTRODUCTION

An improved knowledge of how chemical factors relate to combustion instability has a direct bearing on the choice of propellants as well as chamber design requirements in liquid propellant rocket motors. The time-consuming matching of propellants to chamber design could be shortened through the availability of such knowledge. Also the stability characteristics of space-storable propellants such as liquid methane have a direct bearing on propellant choices for future applications. The ultimate objective of this study was to determine whether the chemical kinetics of the combustion reaction has any bearing upon the incidence or continuation of combustion instability, and if so, to determine the nature of this influence. The relationship of tangential mode spin direction, as well as axial energy release on the transverse modes, have been shown to be associated with the fuel properties. Also, gas rocket studies have verified that well-defined shifts of the unstable regime occur when additives were used to alter the kinetics.

A detailed report on the study of chemical kinetic factors in liquid rocket motors should be available later this year. A summary of that report follows.

DISCUSSION

An experimental investigation of the influence of chemical reaction kinetics upon liquid propellant rocket combustion instability was recently brought to completion. The study sought to determine whether kinetic factors such as induction period, activation energy, and reaction mechanism

influenced the stability of rocket engines, and to investigate whether trends in stability behavior could be predicted on a kinetic basis and whether stability behavior could be influenced by alteration of the kinetic properties of the combustion reaction.

The study was motivated by four factors: first, no study had ever demonstrated conclusively the role of reaction kinetics in the stability behavior of liquid propellant rockets, (note that the dominance of physical transport properties in the combustion in these engines was not being questioned); second, kinetics had been shown to affect stability behavior of rocket engines burning gaseous propellants; third, the opposite preferred spin directions in the first tangential mode of combustion instability of the propellant systems LOX/ethanol and LOX/RP-1 had not been explained by any physical theory, and it was thought that a chemical explanation might be found; and fourth, availability of kinetic research at Princeton University.

Tests were conducted on a 9-inch diameter, liquid propellant motor operating at 150 psia chamber pressure. There were three phases of testing: phase one was an intensive investigation of the stability behavior of the LOX/liquid methane propellant system; phase two was a survey undertaken with LOX and several different fuels to identify any stability trends which might be associated with the variation in kinetic factors among the propellant systems; phase three was direct testing of the propellant system LOX/liquid carbon monoxide to determine whether alterations of explicit kinetic properties by use of additives affected the stability behavior.

Further information on the stability behavior of liquid methane was very desirable because this fuel is being considered for future rocket propulsion systems. Methane

oxidation kinetics are unique among hydrocarbons and are quite different from the kinetics of other fuels as well. Also, comparative data were available from other work going on at Princeton investigating the details of methane oxidation. A study of methane stability in the liquid rocket thus promised much useful design knowledge as well as a chance to correlate peculiarities in its stability behavior with peculiarities in its kinetic parameters.

It was found that the LOX/methane combination had a very high tendency toward spontaneous instability. This instability began upon ignition and quickly reached very high amplitudes (up to 450 psi peak-to-peak). It always occurred in the first tangential spinning mode. Its characteristic preferred spin direction based on an individual element (see Fig.16) was from regions of high fuel concentration to regions of high oxidizer concentration: F→O. Attempts were made to influence this instability by firing a tangential pulse gun into the motor and by varying the length of a three-bladed baffle. Pulsing in either direction did not alter spin direction or change the amplitude. Although shorter lengths decreased amplitude, a three-inch-long baffle was necessary in order to suppress the instability. In contrast, a one-inch-long baffle was sufficient to stabilize the motor with all other fuels tested. Since propellant-displacement theories, and other theories based purely on physical properties, could not explain the unusually high tendency toward instability displayed by this double-cryogenic propellant system, chemical kinetic effects were considered. The kinetic induction period of methane oxidation is known to be unusually long in comparison with those of other fuels (see Fig.17). Also it was found that the induction period depends on the species concentration. The activation energy of methane oxidiation is much higher than those of other fuels. The sensitive zone of the methane

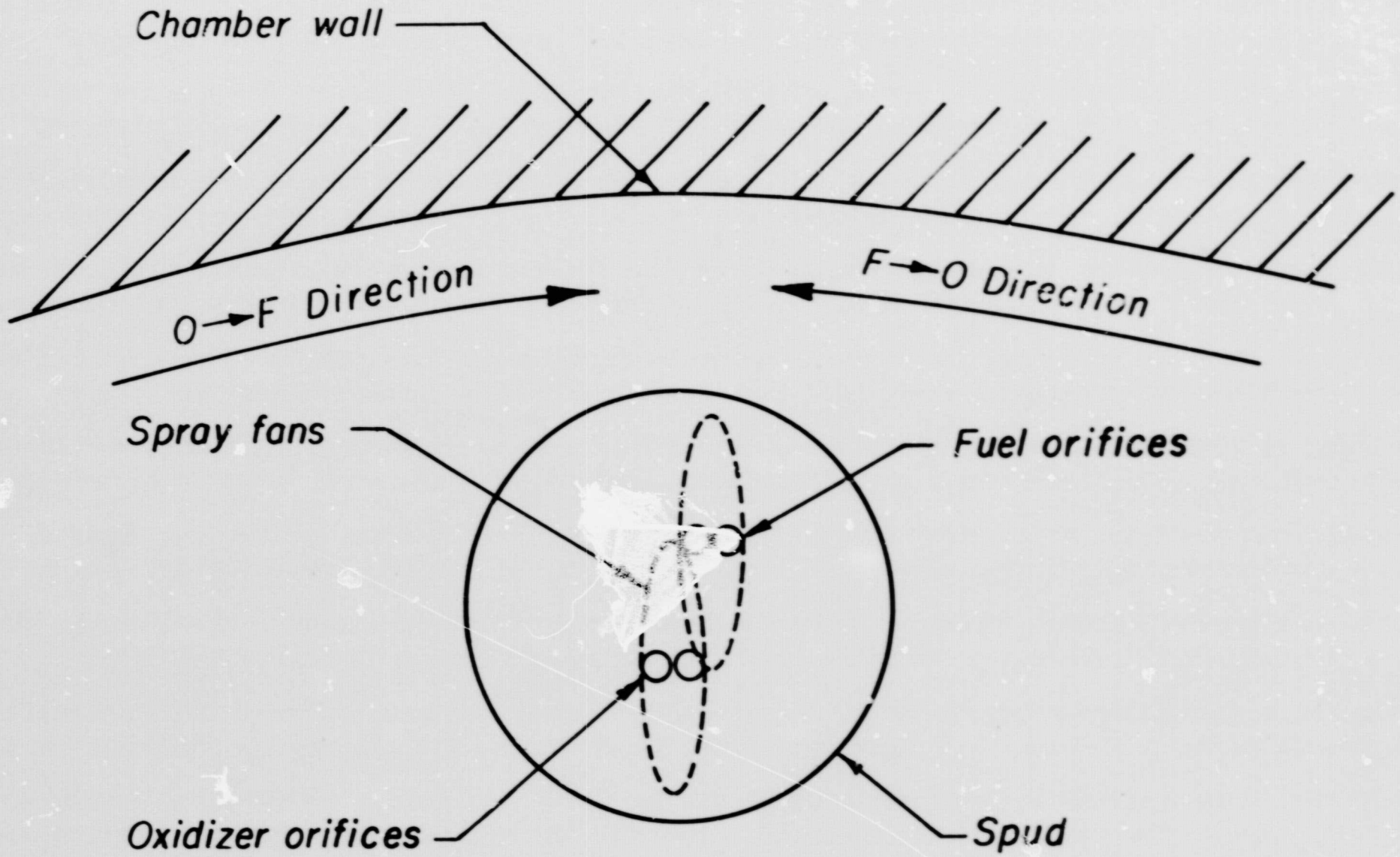

Figure 16

Spud orientation and spin directions

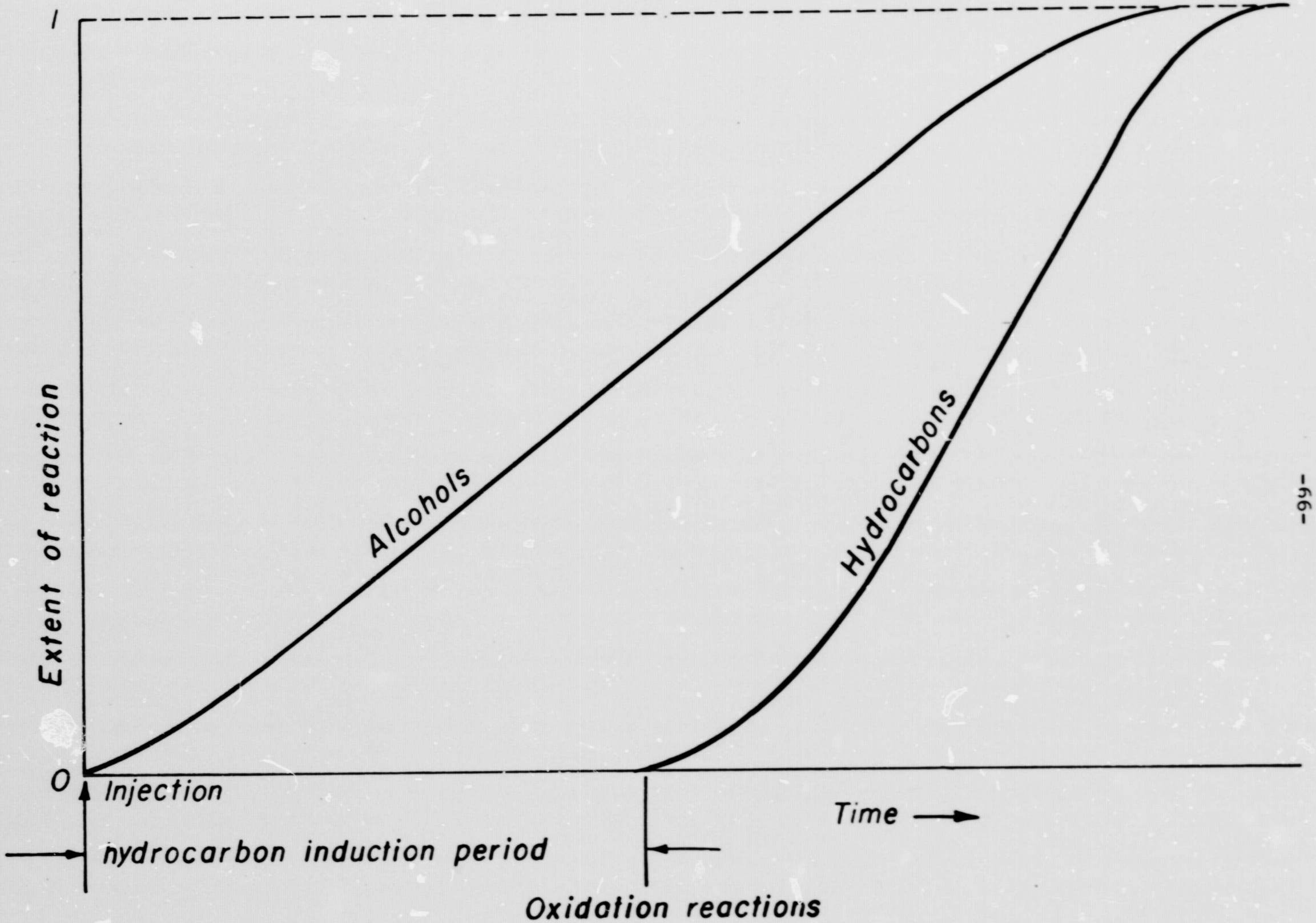
1
Extent of reaction
Alcohols
Hydrocarbons
0
Injection
hydrocarbon induction period
Oxidation reactions
Time

Figure 17

combustion in the baffle tests was clearly further downstream than the sensitive zone of combustion of other fuels. The cryogenic nature of liquid methane seemingly insures that the physical processes of its combustion are not unduly delayed. Thus the singular length of the induction period and the great size of E_{act} were believed to be responsible in some way for the length of the sensitive zone. It was thought also that perhaps kinetic factors could explain the degree of spontaneous instability.

The differences between instability characteristics in ethanol and RP-1 suggested a fuel survey to establish whether these characteristic differences were co-incidental with these particular fuels, or were representative of an intrinsic difference between alcohols and hydrocarbons in their stability behavior. Accordingly, tests were performed using methanol, ethanol, pentane, and RP-1 as fuels.* Under test conditions identical with those of the methane runs, only without the injector changes, it was found that there was a characteristic difference in preferred spin direction between the alcohols and hydrocarbons tested. Instability with alcohol fuels was in the first-tangential mode, spinning in the O→F direction (Fig. 16). Instability with hydrocarbon fuels spun in the F→O direction in the 1-T mode. These preferred spin directions could not be altered by pulsing. In addition, the incidence of spontaneous (linear) instability was somewhat higher with hydrocarbon fuels than with alcohol fuels. Throughout some range in mixture ratio, if linear instability was not present, nonlinear instability could be generated by pulsing. No matter which direction the pulse, the spin direction resulting was the characteristic one for the class of fuel to which the subject fuel belonged. Since conventional instability models could not

*The results of the methane test described above were included in the comparison.

explain the difference in preferred spin direction or the variation in incidence of spontaneous instability between the two types of fuels, kinetic influences which might cause these differences were considered. The oxidations of hydrocarbons (including methane) and alcohols differ in two major respects, which are related. The induction period of hydrocarbon oxidation is significant, while alcohol oxidation exhibits no induction period; and the very important OH radical, which plays a determining role in the chain reaction mechanisms of both oxidations, is present in alcohol fuels, but is not present in hydrocarbon fuels. Thus, there are two kinetic differences between hydrocarbons and alcohols which could account for the characteristic difference in preferred spin direction. The magnitude of the induction period could be associated with a characteristic tangential oscillation frequency which would enhance movement in a preferred direction relative to the induction geometry. The presence or absence of the OH radical in the fuel could couple with concentration gradients in preferred directions. The basic reason for the importance of OH radicals in the fuel molecule is that at the high temperatures of rocket combustion, the first reaction step is a pyrolysis step, cleaving the C-OH bond first in alcohols and the C-C bond in a chain hydrocarbon. Both oxidation of hydrocarbons and of alcohols proceeds by way of hydroxyl radicals in the propagating steps. Alcohols thus produce their own hydroxyl radicals for chain propagation, whereas hydrocarbons must interact with the oxidizer molecules to produce hydroxyl radicals.

The alteration of the kinetics of carbon monoxide by hydrogen and methane additives is well known. In gross terms, the addition of a small amount of hydrogen lowers the overall activation energy, and the addition of a small amount of methane raises the overall activation energy of the carbon monoxide oxidation reaction. The induction period is affected in the

same manner as the activation energy. Basically, these effects result from the modification in the chain mechanism brought about by the additives. The hydrogen reacts with oxygen to produce hydroxyl radicals, which can attack the C≡O triple bond. Because of its high energy, the bond cannot easily be cleaved by pyrolysis alone, and thus propagate the reaction. The methane competes successfully with the CO for the propagative OH radicals and thus keeps the CO oxidation from proceeding.

This knowledge was applied in gas rocket experiments to affect the stability limits in the mixture ratio, chamber length plane (see Fig.18). With CO as fuel, the motor was made more stable by addition of hydrogen and less stable by addition of methane. As no physical properties were altered by the addition of trace amounts of additives, the kinetic effects were isolated as the cause of the stability shifts.

Similar tests were accordingly run on the liquid propellant motor using liquid carbon monoxide as fuel and 1 to 2 percent hydrogen or methane added to alter the kinetics one way or the other from those of pure CO oxidation.

Runs with no additive, that is, pure liquid CO fuel, exhibited only transient spontaneous instability and no pulsed instability. The spontaneous instability lasted for some period of time, of the order of 0.7 sec, and then damped of its own accord (see Fig.19). The duration of the instability and its amplitude both generally correlated together as a function of mixture ratio. The mixture ratio stability history is presented in Fig.20.

Runs with hydrogen additive generally exhibited the same stability pattern as those with no additive. There were a few instances of pulsed instability, but these damped out quickly as shown in Fig.20. However, although the number of

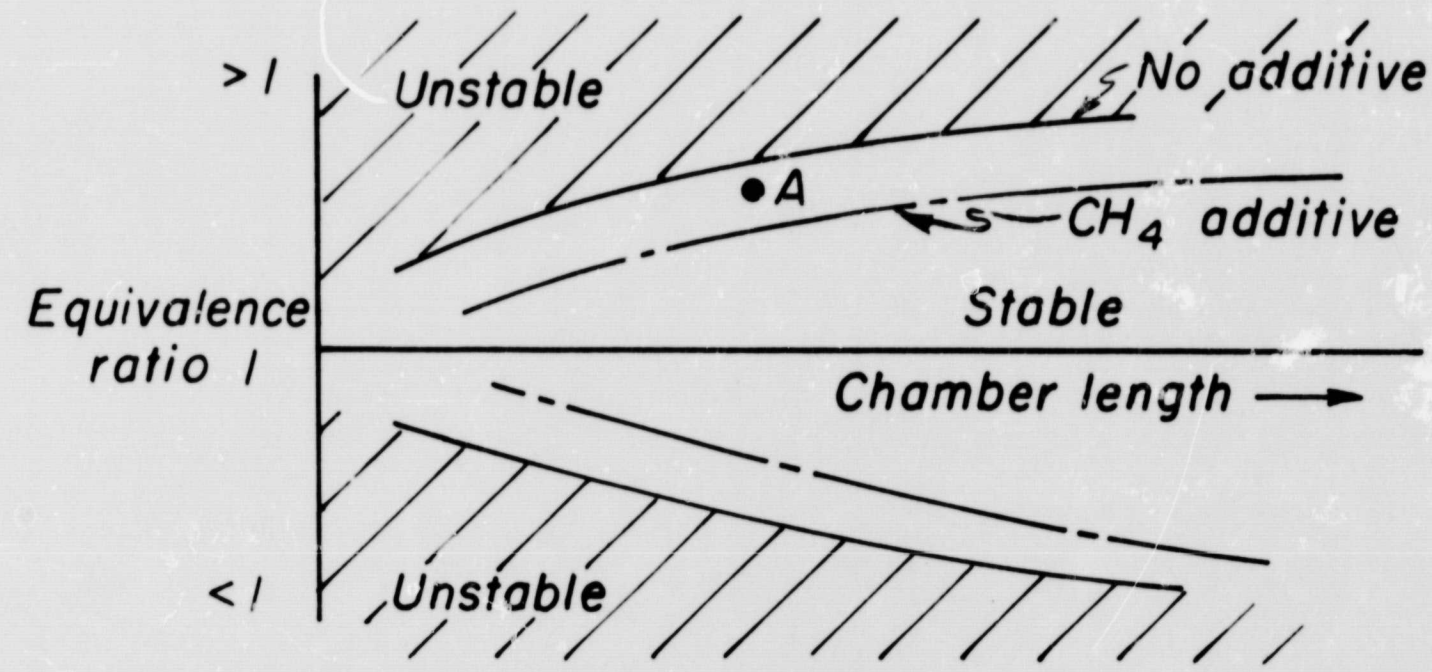

Point A, that was stable with no additive, was unstable with CH_4 additive

Figure 18

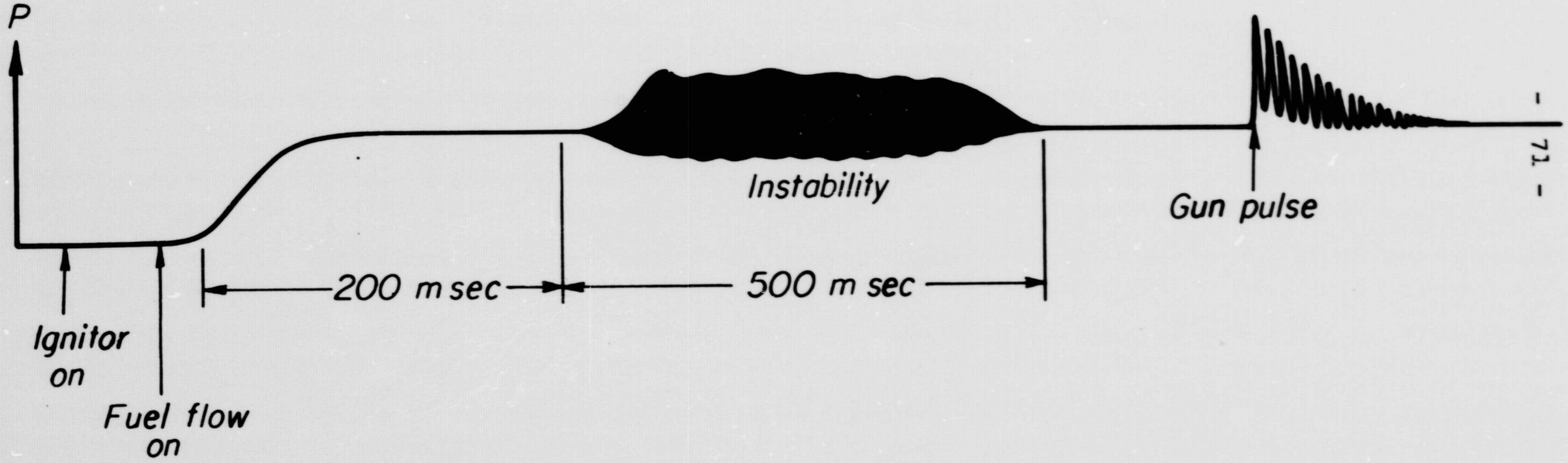

Figure 4 Schematic composite of pressure history of a typical run, LOX/LCO

Figure 19

JP 21 R 4489 70

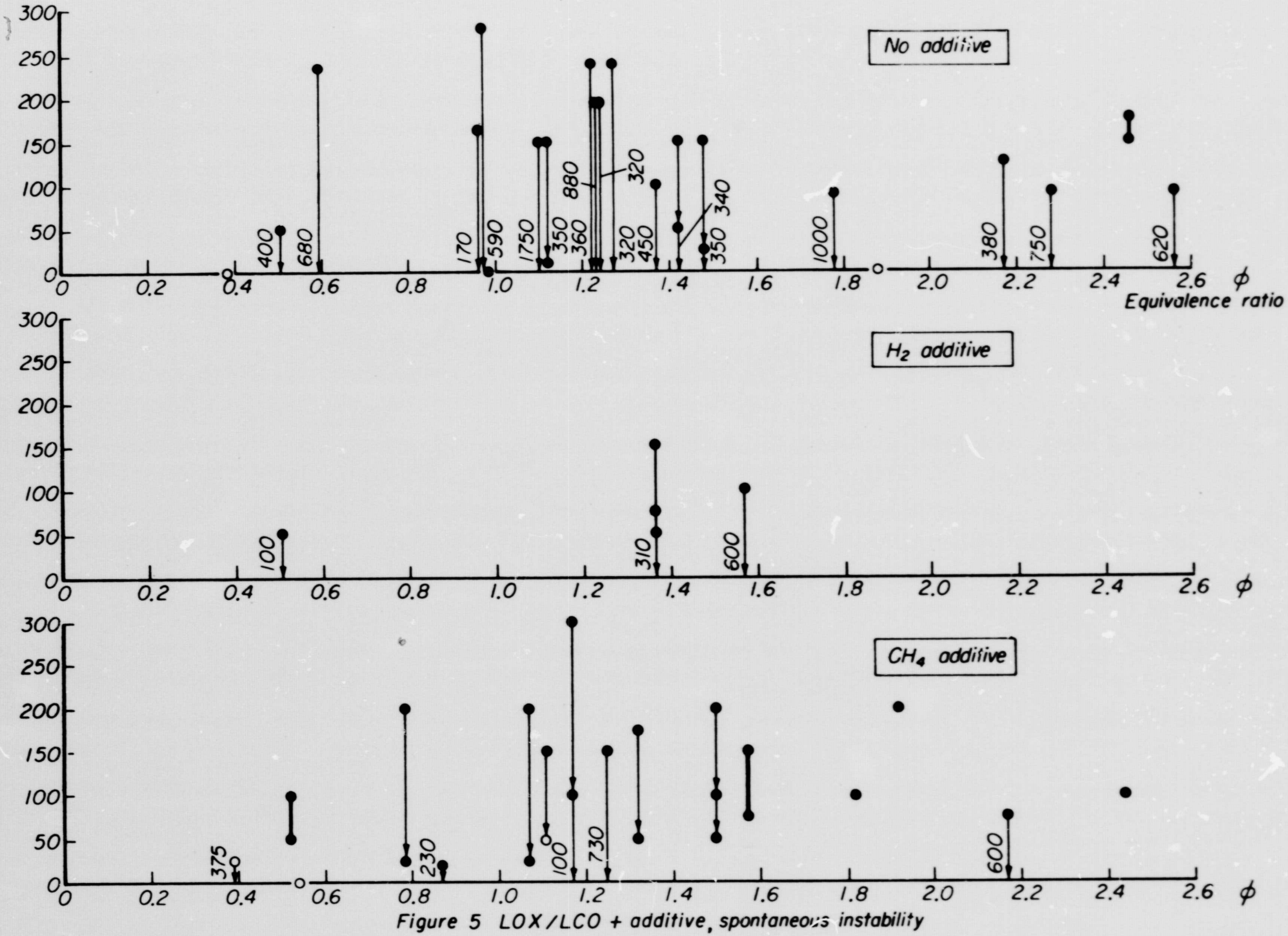

Figure 20

Figure 5 LOX/LCO + additive, spontaneous instability

tests was limited, the spontaneous instability amplitudes were somewhat lower, and the duration considerably shorter, than those of runs at the same mixture ratio without additive.

Runs with methane additive again exhibited generally the same initial stability pattern as those with no additive, but with this noticeable difference: complete damping of the instability rarely occurred (see Fig.20). If damping did occur, it invariably took much longer than did damping at the same mixture ratio with no additive. Thus, addition of methane always increased the duration of spontaneous instability over what it was at the same mixture ratio without additive. Also, any pulsed instability that occurred with methane additive was permanent, in contrast to that observed otherwise, which was transient; and instability amplitudes with methane additive were generally higher than those at the same mixture ratio with hydrogen additive. Methane is seen to have a de-stabilizing effect on the LOX/LCO propellant system.

Thus, the results of these tests on the liquid propellant rocket show the same trends as those on the gas rocket did: hydrogen additive has a stabilizing effect, and methane additive has a de-stabilizing effect upon combustion of carbon monoxide and oxygen. The effects are less significant than in the gaseous system because of the complexity of liquid combustion. But kinetic factors do seem to have an effect on liquid rocket combustion instability.

This study demonstrated that kinetic factors such as activation energy and chain reaction mechanism can play a small part in determining stability behavior of some liquid propellant rocket systems. The additive method may have applications as a way of stabilizing certain marginal engine systems. The study indicated that details in the stability behavior, such as preferred spin direction and relative incidence of spontaneous

instability, may be associated with the chemical nature of the fuel. Also it showed the higher tendency toward instability of the LOX/liquid methane propellant combustion and indicated that care should be taken in designing engine systems for this propellant combination.

X. HYDROGENATION AS AN ENERGY SOURCE

INTRODUCTION

Hydrogenation as an energy source for propulsion was conceived by T. Glassman[20]. Although that preliminary study placed the ultimate emphasis on the acetylene-hydrogen system, the analysis applies equally well to the methyl acetylene-hydrogen system under present consideration. Based on such a theoretical investigation, it was shown that a propulsive system which utilized the hydrogenation reactions for energy release, could possess three characteristics desirable in a rocket motor: high performance, simplicity, and versatility. Before discussing each of these three characteristics with regard to the hydrogen-methyl acetylene system, it is first necessary to further discuss the system itself.

Methyl acetylene is a monopropellant. In a thrust chamber pressurized to twenty atmospheres, it will decompose to the products graphite (fine carbon particles) and hydrogen. The performance based on this mode of operation would be unattractive for propulsive applications. Calculations indicate that the specific impulse would be less than two hundred seconds. The addition of hydrogen, however, offers the possibility that the reaction will be forced to a hydrogenation of the unsaturated hydrocarbon. Ultimately only methane and hydrogen would then be formed as products. Equilibrium calculations reveal that under the influence of twenty atmospheres of chamber pressure, the following reaction marks this product limit:

$$C_3H_4 + 12\ H_2 \rightarrow 3CH_4 + 8\ H_2$$

This energy release occurs at $T_c = 1600^{\circ}F$, with a mean molecular weight of the products, MW = 5.8. Note that the molar mixture

ratio, r_m, equal to the moles of hydrogen per mole of methyl acetylene, is twelve for this point.

The three desirable characteristics mentioned above are easily seen in this system. The liquid propellant rocket achieves high performance primarily because of the low molecular weight exhaust. A simple calculation leads one to expect a characteristic velocity, c*=6500 ft/sec, for this propellant. The simplicity is achieved through the low chamber temperature involved. No special cooling is then necessary since readily available metals have melting points greater than the operating temperature. The versatility of the system is in the ability to afterburn the exhaust products. Such a device is a natural starting point for the ram-rocket concept. If all three characteristics evolved into an operational device, it would warrant further investigation.

EXPERIMENTAL PROGRESS

The preceding discussion has outlined the development of the hydrogenation concept. An experimental program to investigate the validity of the concept has been in progress over these past months. Following the necessary test stand revisions to handle the experimental apparatus the feasibility testing was initiated. Throughout the testing, the basic configuration of the motor has remained constant as shown in Fig. 21. The thrust chamber is tubular, being three inches in diameter and one foot in length. The nozzle is a standard DeLaval nozzle formed from a carbon block.

Two injection patterns were tested in the motor. The first was an unlike-triplet injector with two jets of hydrogen impinging on a central jet of methyl acetylene. It was not possible to sustain any reaction using this injector. Oxygen-enriched combustion did occur but was terminated when the oxygen was reduced and the hydrogen added. The second injector consisted of a centrally located, solid cone oil burner nozzle

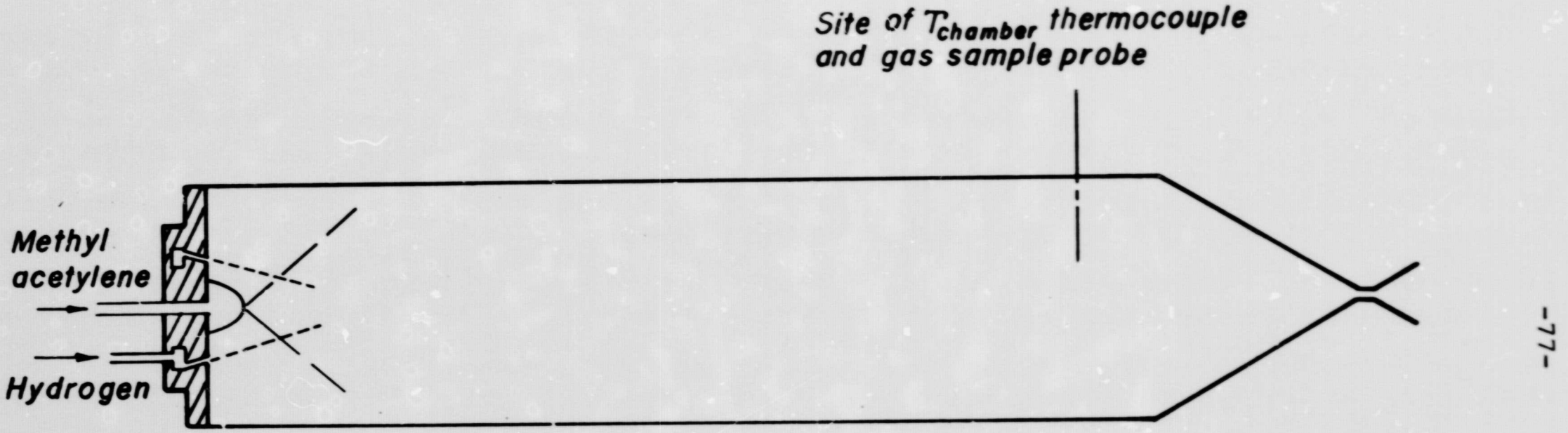

Figure 21

Monopropellant Rocket Used to Study Hydrogenation

to spray the methyl acetylene into the chamber. Hydrogen jets impinged on this 80° conical spray surface from a ring of surrounding showerhead jets. Using this injector, methyl acetylene decomposition was achieved and the addition of hydrogen did not terminate the reaction. Although a molar mixture ratio equal to the theoretical optimum value of twelve has not yet been attempted, a value $r_m = 5.2$ has been achieved.

Further testing was halted temporarily while product gas sampling instrumentation was being designed, constructed, and installed. The performance at $r_m = 5.2$ was calculated from measured data as c* = 5300 ft/sec; chamber temperature was measured at $T_c = 2150\ ^oF$. This performance is in comparison to c* = 2700 ft/sec for the monopropellant case. Such an increase can be attributed to either of two mechanisms: (1) the hydrogenation reaction is proceeding, at least in part, yielding gaseous products of a lower molecular weight; (2) the hydrogen is behaving as a working fluid for the methyl-acetylene decomposition. Of course, a combination of these two is also possible. Although neither alternative has been verified, the appearance of the exhaust products tends to favor the second mechanism for increased performance. It is expected that the gas sampling will clarify the situation.

CONCLUSIONS

Perhaps the most significant result of the experimental program to check the hydrogenation concept is that a reaction can be sustained in the motor with significant amounts of hydrogen addition. This has been accomplished in an extremely simple rocket design, a tube serving as the chamber, an oil burner spray nozzle and surrounding showerhead orifices providing for the propellant injection. The exhaust products,

based upon visual observation, appear to be fine carbon particles and hydrogen rather than the methane-hydrogen exhaust hoped for with hydrogenation taking place. Gas sampling will confirm this preliminary observation. Even with the present exhaust products relatively high performance, low chamber temperature and combustible exhaust products result. These characteristics appear attractive for ram-rocket type applications.

XI. CONCLUDING REMARKS

The admittance coefficient for a surface acoustically-lined by means of Helmholtz resonators may now be calculated from first principles without any need for empiricism. A logical design procedure follows from these calculations. The theory and calculations are now being extended to situations where the dimensions of the resonator cavity become significant compared to the wavelength. Preliminary experimental results indicate a verification of the acoustic liner theory.

Experimental and theoretical results using a diffusion flame model indicate that the response of the wake of a burning droplet to velocity oscillations may be large enough to drive combustion instability. Another theoretical study indicates the thermal response of the condensed phase in a burning droplet may be a significant factor in the feedback mechanism which results in combustion instability. Further experimental and theoretical studies should lead to an injection design procedure which would minimize the occurrence of combustion instability.

A simplified mathematical approach has been developed which allows the analysis of transverse wave behavior in rocket chambers. This would ultimately lead to prediction of nonlinear instability with or without shock waves.

A method has been developed by which steady-state burning rates can be accurately determined for any given propellant combination. For each propellant combination static pressure measurements are employed on a limited number of selected engine configurations. This ultimately leads to accurate steady-state engine design. The information obtained does also form the basis for more accurate instability studies. The method is presently being applied to the study of unsteady combustion.

Studies with liquid CO, methane, and higher order hydrocarbons have shown that some secondary stability characteristics are affected by chemical kinetic factors: travelling transverse waves spin in the oxidizer-to-fuel direction for alcohol but in the opposite direction for hydrocarbons; methane (with its long chemical induction time) requires longer baffles for stabilization; the stability characteristics of liquid CO are altered in opposite ways by the addition of small amounts of H_2 and CH_4 but consistently with their effects on CO kinetics; and a variety of other effects are noticed.

Acetylenic monopropellants could be made to decompose in rocket chambers in the presence of a large excess amount of hydrogen in order to increase the performance of both rockets and afterburners. However, little evidence was obtained to show that the rocket exhaust contained substantial amounts of methane which would have given optimum performance.

NOMENCLATURE

a	Velocity amplitude (see Eq. (9), Sect. III)
A	Orifice cross-sectional area
A_2, B_2	Velocity amplitudes at the tube entrance (Sect. IV)
b	Chamber velocity amplitude in phase with chamber pressure (see Eq. (8), Sect. III)
b	Flame width (Sect. VI)
c	Speed of sound
c_p	Specific heat of gases
C_D	Discharge coefficient
C_p	Pressure coefficient
C_1	Defined as $\cos(\sigma_1 + \sigma_2)$, (Sect. IV)
C_1, C_2, C_3	Constants of integration (Sect. VI)
d_0	Initial diameter of jet (Sect. VI)
f	Frequency
g	Chamber velocity amplitude out-of-phase with chamber pressure (see Eq. (8), Sect. III)
G	Defined in Eq. (1), Sect. VIII, related to the in phase energy addition in the combustion chamber
h	Static enthalpy
k	Pre-exponential factor in the Clausius-Clapeyron Law
K, K^*	Vaporization rate constants
ℓ	Length of quarter-wave tube
L	Length of resonator orifice
$\mathcal{L}$	Latent heat of fuel
$\dot{m}$	Evaporation mass flux
M_r	Defined as $M_r = \bar{U}_r/c_\infty = U_0 - U_\infty / c_\infty$
M_{rel}	Relative Mach number $M_{rel} = \bar{V}_e/\bar{c}$

p	Pressure
Pr	Prandtl number
q	Combustion heat release per unit mass of oxidizer consumed
r	Drop radius
$\mathcal{r}$	Radial coordinate (Sect. VI) Local evaporation rate of droplet (Sect. VIII)
$\mathcal{r}_o$	Initial radius of jet (Sect. VI)
R	Transformed radial coordinate
$\mathcal{R}$	Fractional evaporation rate (without $e^{i\omega\tau}$ part)
Re	Reynolds number
S	Strouhal number = $\omega \mathcal{r}_c/\nu$
S_1	Defined as $\sin(\alpha_1 + \alpha_2)$ (Sect. IV)
t	Time
T	Temperature
u	Axial velocity component (Sect. VI) Relative velocity $u = V_1 - V_2$ (Sect. VIII) Gas velocity in quarter-wave tube (Sect. IV)
$\hat{u}$	Orifice velocity amplitude (Sect. III)
U_∞	Velocity of external stream (Sect. VI)
v	Radial velocity component (Sect. VI)
V	Gas velocity
$\mathcal{v}$	Volume of resonator cavity
W	Defined by Eq.(2), Sect. IV
x	Axial space coordinate
Y	Mass fraction of species
$\mathcal{y}$	Admittance
z	Axial distance measured from the injector end (Sect. VIII)

Z	Impedance
α	Defined as $(i\ Re\ S)^{-1/2}$ (Sect. VI)
α	Thermal diffusivity of the droplet (Sect. VIII)
β	Shvaab-Zeldovich enthalpy variable
γ	Ratio of specific heats
Γ_i	Shvaab-Zeldovich variable for mass concentration of species i
δ	Phase angle
ϵ	Oscillation amplitude (see Eq. (5), Sect. III and Eq. (1), Sect. VI)
η	Transformed radial coordinate
κ	Constant defined by Eq. (3), Sect. III
λ	Wavelength
μ	Molecular viscosity
ν	Molecular kinematic viscosity
ξ	Transformed axial coordinate
ρ	Gas density
σ	Percent open area ratio of lined surface
τ	Transformed time coordinate
ψ	Angle between $\vec{\bar{V}}_1$ and $\vec{V}_1'$ when both vectors are considered positive (Sects. III and IV)
ω	Angular frequency
$\tilde{\omega}$	Nondimensional angular frequency where $\tilde{\omega} = \omega L/\bar{c}_1 = 2\pi L/\lambda$ (Sect. III)
$\ddot{\omega}$	Nondimensional angular frequency where $\ddot{\omega} = \omega\alpha/\kappa^2$

Subscripts

c	Centerline of flame (Sect. VI)
e	External flow
i	Species i
I	Imaginary part
M	Enthalpy and mass concentration distributions
o	Per unit orifice area, e.g., R_o (Sect. III) Value at initial section (Sect. VI) Center condition of the droplet (Sect. VIII)
O	Oxidizer
r	Resonant condition
R	Real part
w	Liquid surface (Sect. VIII)
W	Axial velocity distributions (Sect. VI)
1	Pertaining to chamber
2	Pertaining to entrance
∞	Value in the external stream

Superscripts

$\bar{(\ )}$	Mean or steady-state value
$\overset{=}{(\ )}$	Mean value due to nonlinear effects of oscillations (Sect. VI)
$(\ )^*$	Dimensional variable
$(\ )'$	Perturbation
$\vec{(\ )}$	Vector
$(\ )^+$	Inward flow
$(\ )^-$	Outward flow
$\hat{(\ )}$	Transformed dependent variables

REFERENCES

1. Crocco, L., Harrje, D. T., Sirignano, W. A., et al, "Nonlinear Aspects of Combustion Instability in Liquid Propellant Rocket Motors - Sixth Yearly Progress Report," Princeton University Dept. of Aerospace and Mechanical Sciences Rept. 553f, June 1966.

2. Tonon, T. S. and Sirignano, W. A., "Near-Resonant, Off-Resonant, and Quasi-Steady Theories of Acoustic Liner Operation," Sixth ICRPG Combustion Conference, CPIA Pub. No. 192, Vol. 1, Dec. 1969, pp. 249-256.

3. Tonon, T. S. and Sirignano, W. A., "The Nonlinearity of Acoustic Liners with Flow Effects," AIAA Paper No. 70-128, AIAA Eighth Aerospace Sciences Meeting, Jan. 1970.

4. Tonon, T. S. and Sirignano, W. A., "Nonlinear Theories on Acoustic Liner Operation with Flow Effects," Princeton University Dept. of Aerospace and Mechanical Sciences, Rept. No. 885, 1970.

5. Cantrell, R. H. and Hart, R. W., "Interaction Between Sound and Flow in Acoustic Cavities: Mass, Momentum, and Energy Considerations," J. Acoustical Soc. Amer., Vol. 36, No. 4, 1964, p. 697.

6. Bracco, F. V., "On the "Direct" Method and Its Application to Certain Combustion Problems,", Ph.D. Thesis, Princeton University Dept. of Aerospace and Mechanical Sciences Report #902, 1970.

7. Bracco, F. V. and Harrje, D. T., "The Direct Method Applied to Steady Liquid Propellant Combustion: Investigation of Several Droplet Burning Models for a LOX/Ethanol Engine," Sixth ICRPG Combustion Conference, CPIA Pub. No. 192, Dec. 1969, pp. 65-91.

8. Crocco, L., "Theoretical Studies on Liquid Propellant Rocket Instability," Tenth Symposium (International) on Combustion, The Combustion Institute, 1965, p. 1101.

9. Strahle, W. C., "Unsteady Laminar Jet Flame at Large Frequencies of Oscillation," AIAA J. Vol. 3, No. 5, May 1965, p. 957.

10. Feiler, C. E. and Yeager, E. B., "Effect of Large Amplitude Oscillation on Heat Transfer," NASA TR R-142, 1962.

11. Lemlich, R. and Hwu, C. K., "The Effect of Acoustic Vibration on Forced Convective Heat Transfer," A. I. Ch. E. Journal, Vol. 7, March 1961, pp. 102-106.

REFERENCES - CONT'D

12. Bogdanoff, D. W., "A Study of the Mechanisms of Heat Transfer in Oscillating Flow," Princeton University Dept. of Aerospace and Mechanical Sciences Rept. 483-f, Oct. 1967.

13. Chervinsky, A. P., Sirignano, W. A., Harrje, D. T., and Varma, A. K., "Axisymmetric Jet Diffusion Flame in an External Oscillating Stream, Sixth ICRPG Combustion Conference, CPIA Pub. No. 192, Vol. 1, Dec. 1969, pp. 171-180.

14. Chervinsky, A. P. and Sirignano, W. A., "The Effect of High Frequency Periodic Oscillations on Axisymmetric Wake Diffusion Flames", AIAA Paper No. 70-10, AIAA Eighth Aerospace Sciences Meeting, Jan. 1970.

15. Priem, R. J. and Heidmann, M. F., "Propellant Vaporization as a Design Criterion for Rocket-Engine Combustion Chambers," NASA TR R-67, 1960.

16. Strahle, W. C., "A Theoretical Study of Unsteady Droplet Burning: Transients and Periodic Solutions," Ph.D. Thesis, Princeton University Aero. Eng. Rept. No. 671, 1963.

17. Williams, F. A., "Response of a Burning Fuel Plate to Sound Vibration," AIAA J., Vol. 3, 1965, p. 2112.

18. Wise, H., and Ablow, C. M., "Burning of a Liquid Droplet, III. Conductive Heat Transfer within the Condensed Phase during Combustion", J. Chem. Phys. 27, 2 Aug. 1957.

19. Crocco, L., and Cheng, S. I., "Theory of Combustion Instability in Liquid Propellant Rocket Motors, AGARDograph No. 8, Butterworths Sci. Pub. Ltd., London, 1956.

20. Glassman, I., "Method of Producing Thrust by Hydrogenation of an Acetylenic Hydrocarbon,", U.S. Patent No. 3,170, 281.